



Is the exhumation of the Sierras Pampeanas only related to Neogene flat-slab subduction? Implications from a multi-thermochronological approach

Frithjof A. Bense*, Stefan Löbens, István Dunkl, Klaus Wemmer, Siegfried Siegesmund

Geoscience Centre, University of Göttingen, Goldschmidtstraße 3, 37077 Göttingen, Germany



ARTICLE INFO

Article history:

Received 16 June 2013

Accepted 3 September 2013

Keywords:

Sierras Pampeanas

Thermochronology

(U–Th)/He dating

Apatite fission-track

Exhumation

ABSTRACT

This paper presents new thermochronological data and reviews a set of recently published data for the Sierras Pampeanas in central and northwestern Argentina, which constitutes a distinct morphotectonic feature between 27°S and 33°S. Thermochronological data, derived from zircon and apatite (U–Th)/He, as well as apatite fission-track dating, reveal that cooling below 200 °C commenced locally during the Carboniferous period. In Permo-Triassic times, pronounced cooling propagated from east to west in the Southern Sierras Pampeanas, being time-equivalent and spatially equivalent to a flat-slab subduction period at these latitudes. Mesozoic rifting, accompanied by sedimentation and burial re-heating, only affected the thermal history of sampled rocks locally, suggesting that substantial sedimentary thicknesses were only accumulated along narrow and spatially-restricted Cretaceous rift basins. Final cooling in the northern Pampean ranges occurred during the Miocene. Contrastingly, in the Southern and Southwestern Sierras Pampeanas, cooling to near-surface temperatures occurred between the Late Cretaceous and the Paleogene, supporting the idea that a positive topography already existed in these areas before the Neogene. This contradicts the previous hypothesis that the uplift of the Pampean ranges is completely related to the Neogene flat-slab subduction. Instead, this process just accentuated a pre-existing relief built up by diachronously developed Mesozoic land surfaces. Calculated long-term denudation rates, varying between 0.010 and 0.024 km/Ma, also support the idea of diachronous surfaces preserved since Mesozoic times.

© 2013 Elsevier Ltd. All rights reserved.

1. Introduction

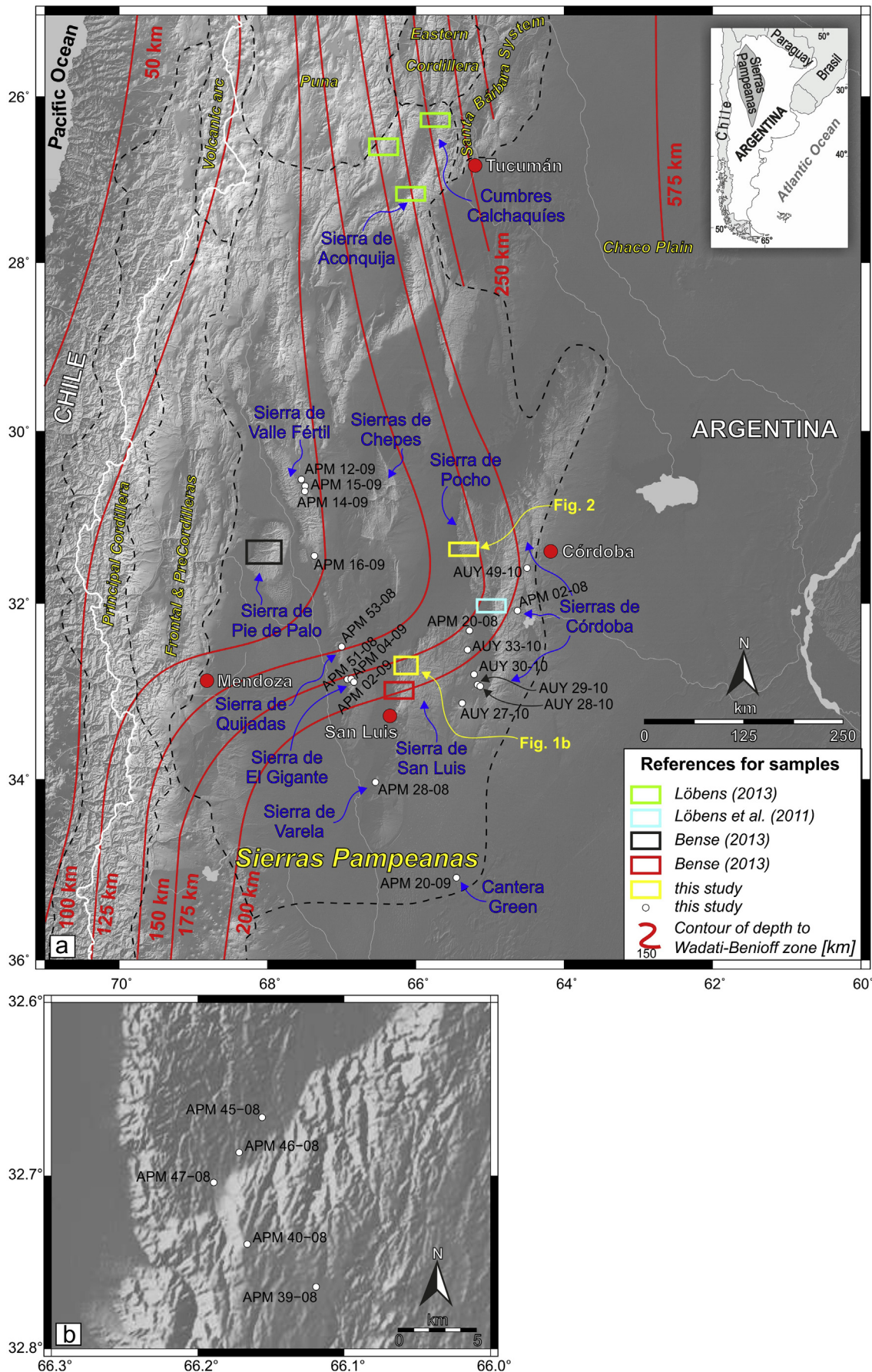
Thermochronological dating methods such as apatite fission-track (AFT) as well as (U–Th)/He zircon and apatite dating (ZHe & AHe) are appropriate for investigating the thermal evolution of the upper crust below ~200 °C (e.g. Farley and Wolf, 1996). Integration of this thermal evolution of basement blocks with information from the sedimentary record of the surroundings can be used to constrain the thermal and tectonic evolution of the shallow crust (e.g. Gallagher et al., 1998; Farley, 2002; Ehlers and Farley, 2003; Löbens et al., 2011).

The Sierras Pampeanas in central and northwestern Argentina constitute a morphotectonic region of several roughly north–south trending mountain ranges (Fig. 1) separated by inter-mountain basins (e.g. González Bonorino, 1950; Caminos, 1979; Jordan and

Allmendinger, 1986; Ramos et al., 2002). The study area is composed of twelve major Pampean basement blocks (Fig. 1) consisting of Neoproterozoic to Early Paleozoic igneous and metamorphic rocks (e.g. González Bonorino, 1950; Caminos, 1979; Gordillo and Lencinas, 1979). Those ranges were affected by Early Cenozoic crustal shortening (e.g. Benjamin et al., 1987; Noble et al., 1990; Carrapa et al., 2011) related to the westward subduction of the Nazca Plate beneath the South American Plate. Deformation results in a thick-skinned thrust belt (Jordan and Allmendinger, 1986), characterized by i) the uplift of the eastern margin of the Puna Plateau in the northern part of the Pampean ranges (Isacks, 1988; Jordan and Alonso, 1987) and ii) presumably the uplift of the Sierra de Pie de Palo in the Western Sierras Pampeanas (Löbens, 2013) at that time. During the Neogene, the incorporation of the aseismic Juan Fernández Ridge into the subduction generated a flattening of the subduction angle in the area of 27–33°S (e.g. Barazangi and Isacks, 1976; Pilger, 1981; Jordan et al., 1983; Yáñez et al., 2001). This flat-slab subduction is interpreted to have caused the exhumation and uplift of the individual Pampean

* Corresponding author.

E-mail addresses: fbense@geo.uni-goettingen.de, fbense@gwdg.de (F.A. Bense).



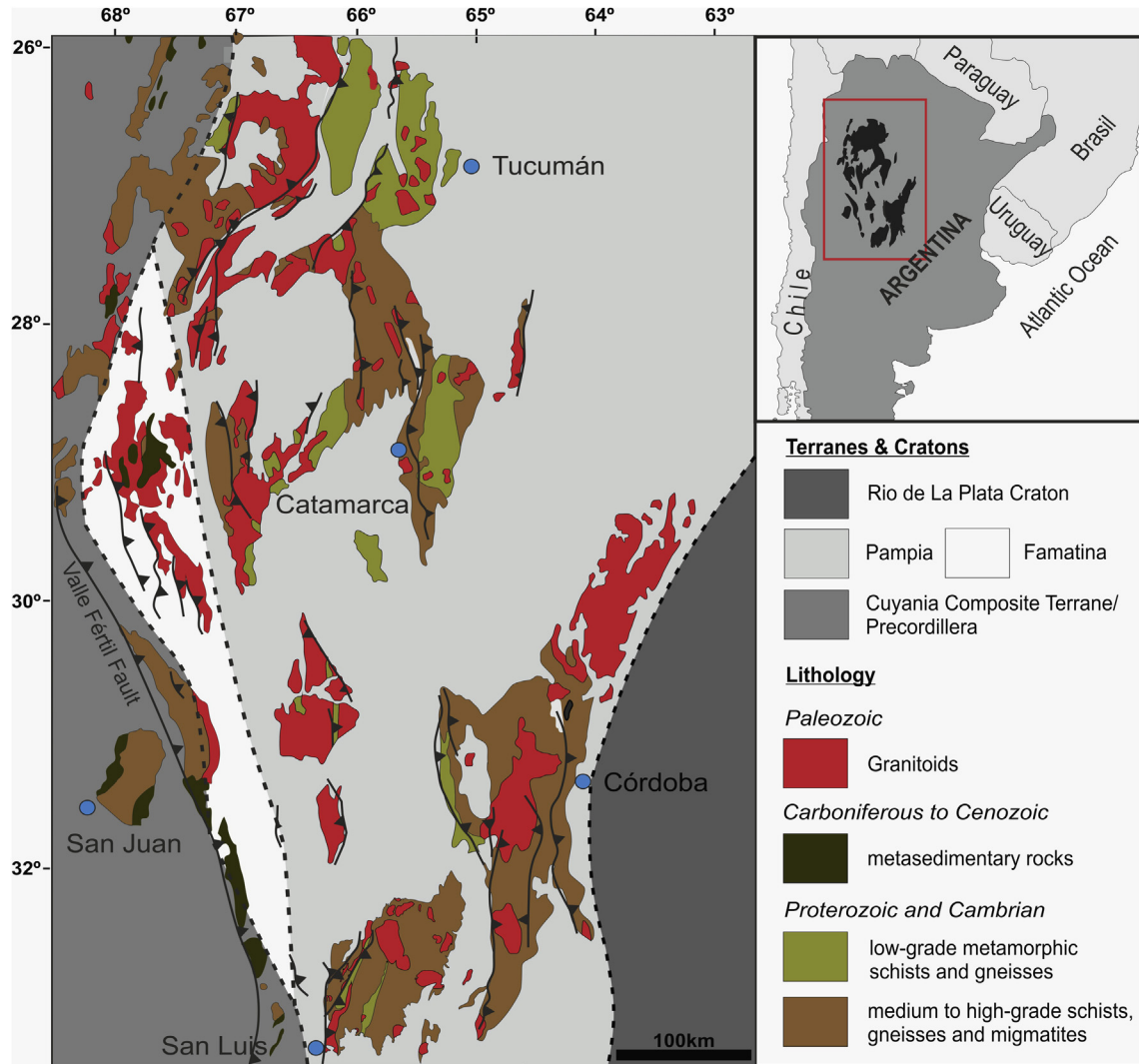


Fig. 2. Simplified geological sketch map of the Sierras Pampeanas. Dashed lines indicate inferred position of Precambrian to Paleozoic terrane boundaries (modified according to Ramos, 2010; based on van Gosen, 1998). Also indicated are the individual Pampean basement-block uplifts and associated bounding faults. Major fault vergence based on González Bonorino (1950) and Jordan and Allmendinger (1986).

mountain ranges (see e.g. Dávila and Carter, 2013) as well as to have determined the type of deformation within the Sierras Pampeanas by reactivating and inverting major Late Proterozoic and Early Paleozoic crustal discontinuities during Andean deformation (e.g. Jordan et al., 1983; Yañez et al., 2001).

Exhumation processes can be qualitatively and quantitatively constrained by integrated cooling paths, which enable the development of time-dependent structural and surficial evolutionary models for a region. So far, those models exist either for individual mountain ranges within the Sierras Pampeanas (e.g. Sobel and Strecker, 2003; Mortimer et al., 2007; Löbens et al., 2011), are only based on thermochronological data lacking modelled time–temperature paths (Jordan et al., 1989) or use only one thermochronological system (Dávila and Carter, 2013). Therefore, the aim of this paper is to combine those evolutionary models of basement ranges from the Eastern, Western, and Northern Sierras Pampeanas with new apatite fission-track and zircon and apatite (U–Th)/He cooling ages, in order to develop a time-dependent cooling model for the whole Sierras Pampeanas.

1.1. Regional geology of the Sierras Pampeanas

The Sierras Pampeanas in central and northwestern Argentina constitute several mountain ranges representing individual tectonic blocks of crystalline basement. Basement is mainly characterized by metamorphic and granitic rocks, e.g. low-to-medium-grade schists, amphiboles, and gneisses (e.g. González Bonorino, 1950; Caminos, 1979; Gordillo and Lencinas, 1979), formed during the accretion of different allochthonous and parautochthonous terranes during the Pampean, Famatinian, and Achalian Orogeny in Late Proterozoic to Middle Paleozoic times (Fig. 2). The tectono-metamorphic evolution and associated ductile deformation of the basement is considered to have been completed by Early Carboniferous times (e.g. Ramos, 1988; Ramos et al., 2002; Steenken et al., 2004; Miller and Söllner, 2005; Ramos, 2008).

During Late Paleozoic to Mesozoic times, the deposition of non-marine strata occurred (Fig. 3). The Upper Paleozoic to Lower Mesozoic strata of the Paganzo basin (e.g. Gonzalez and Aceñolaza, 1972), which formed due to extension during the

Fig. 1. a) SRTM3 digital elevation model of the Sierras Pampeanas showing locations of samples discussed in this study; black dashed lines mark boundaries of tectonic provinces according to Hilley and Coutand (2010). Depth of Wadati–Benioff zone according to Cahill and Isacks (1992). b) Magnification of the San Francisco del Monte de Oro area.

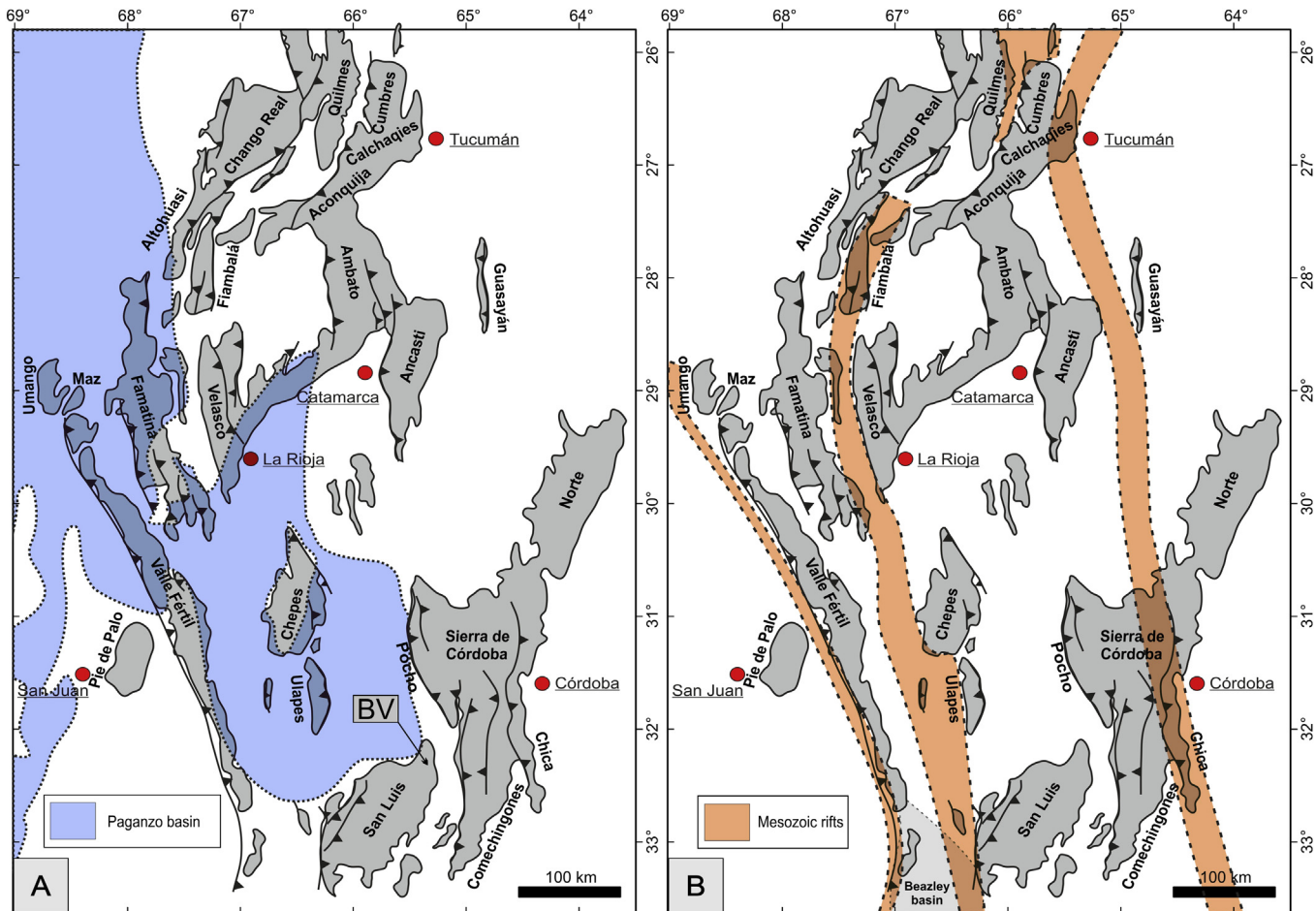


Fig. 3. A) Late Paleozoic Paganzo basin with main depocentres (based on Salfity and Gorustovich (1983) and Koukharsky et al. (2001), modified from Ramos et al., (2002). B) Location of major rift systems of Triassic–Early Jurassic and Early Cretaceous ages (modified from Ramos et al., 2002). BV: Bajo de Véliz.

orogenic collapse following the Early Paleozoic orogenic mountain building (Mpodozis and Ramos, 1990; Ramos et al., 2002), is mainly restricted to the southwestern parts of the Sierras Pampeanas (Salfity and Gorustovich, 1983). During the Mesozoic, two rift events affected the basement of the Sierras Pampeanas and reactivated older crustal discontinuities, leading to an irregular cover of non-marine sediments atop the basement with variable but, locally, up to 5000 m thickness (Fig. 2; e.g. Jordan et al., 1983; Schmidt et al., 1995). The first extensional event occurred during Late Triassic to Early Jurassic times. It led to the deposition of non-marine sediments in localized depocenters. They were mainly located along a NNW-trending series of basins, i.e. along the Valle Fértil fault in the western part of the Sierras Pampeanas, e.g. the Ischigualasto, Marayes, Las Salinas, and Beazley basins (Figs. 2 and 3; Criado Roque et al., 1981; Aceñolaza and Toselli, 1988; Ramos et al., 2002).

The second extensional event occurred during Early Cretaceous times, associated with the opening of the South Atlantic Ocean at these latitudes (Fig. 2; Schmidt et al., 1995; Rossello and Mozetic, 1999). Major but narrow rift basins developed along the eastern and western borders of the Pampia terrane, e.g. along the western side of the Sierra Chica de Córdoba and Valle Fértil. These basins contain accumulated sediment thicknesses of up to 2000–2500 m (e.g. Santa Cruz, 1979; Gordillo and Lencinas, 1979; Criado Roque et al., 1981; Battaglia, 1982; Jordan et al., 1983; Schmidt et al., 1995; Gardini et al., 1996, 1999; Costa et al., 2000, Costa et al. 2001a,b; Ramos et al., 2001, 2002). Due to subsequent erosion,

the original extent of those Mesozoic depocenters is not well known (Furque, 1968; Gonzalez and Aceñolaza, 1972; Lucero Michaut and Olsacher, 1981; Ramos, 1982; Salfity and Gorustovich, 1983; Jordan et al., 1983). However, the quite asymmetrical patterns of Mesozoic cover sediments indicate that large areas of the Central and Eastern Sierras Pampeanas had little or no sedimentary cover (e.g. Jordan et al., 1983; Schmidt et al., 1995; Löbens et al., 2011).

During Miocene times (18–11 Ma), the Juan Fernández Ridge was incorporated into this subduction of the Nazca Plate beneath the South American Plate (e.g. Gutscher et al., 2000; Yáñez et al., 2001). The collateral shortening and flattening of the subduction angle (Stauder, 1973; Barazangi and Isacks, 1976; Pilger, 1984) is interpreted to have led to a reactivation and inversion of the Mesozoic extensional fault systems, causing uplift and deformation of the Pampean basement blocks. The geometry of these reverse faults and thrusts is mainly determined by the orientation of the older Late Proterozoic to Paleozoic structures, resulting in a dominance of east-dipping structures (Fig. 2). The preferred fault orientation is also morphologically expressed by the distinct asymmetry of the Pampean basement blocks. Generally, the ranges show a steeply dipping, fault-facing western slope in contrast to a gently dipping slope on the fault-averted eastern side (González Bonorino, 1950; Gordillo and Lencinas, 1979; Criado Roque et al., 1981; Gonzalez Diaz, 1981; Jordan and Allmendinger, 1986; Introcaso et al., 1987; Massabie, 1987; Costa and Vita-Finzi, 1996; Ramos et al., 2002).

Table 1
Zircon and apatite (U–Th)/He data.

Location	Sample ID (Lithology)	Coordinates [DD.dd]	Altitude [m]	He [ncc]	s.e. [%]	U238 mass [ng]	s.e. [%]	Th232 mass [ng]	s.e. [%]	Th/U	eU [ppm]	Sm mass [ng]	s.e. [%]	Used Ft-corr.	Uncorr. age [Ma]	Ft-corr. age [Ma]	2s [Ma]	Mean age [Ma]
<i>Zircon</i>																		
Sierra de Córdoba	APM 02-08 (migmatite)	-64.63000 -32.08067	805	15.023 80.195 32.439	1.7 1.6 1.6	0.666 2.411 0.998	1.8 1.8 1.8	0.125 0.862 0.345	2.4 2.4 2.4	0.19 0.36 0.35	88.9 413 178.3	0.029 0.276 0.059	22 21 22	0.76 0.82 0.84	176.2 248.4 243.6	176.2 248.4 243.6	8.3 11.4 11.3	222.7
Santa Rosa de Calamuchita																		
Conlara valley	APM 20-08	-65.276500	631	143.775	1.6	5.01	1.8	1.191	2.4	0.24	703.9	0.246	10	0.79	220.83	278.74	21.67	264.2
Santa Rosa de Conlara		-32.310166		66.673 37.967 67.277	1.6 1.6 1.6	3.04 1.25 2.60	1.8 1.8 1.8	0.790 0.485 0.342	2.4 2.4 2.4	0.26 0.39 0.13	766.2 217.6 742.9	0.161 0.030 0.040	10 10 10	0.76 0.79 0.75	168.58 226.21 203.81	222.23 284.54 271.54	19.12 21.86 24.01	
Sierra de Varela	APM 28-08 (gneiss)	-66.54650 -34.03100	548	82.134 39.851 62.310 166.147	1.6 1.6 1.6 1.6	2.899 2.185 4.025 7.633	1.8 1.8 1.8 1.8	0.628 0.187 0.549 1.017	2.4 2.4 2.4 2.4	0.22 0.09 0.14 0.13	492.3 757.1 1257.2 722.4	0.217 0.152 0.530 0.869	6 20 20 5	0.79 0.74 0.74 0.83	218.9 146.1 122.8 172.0	276.4 197.7 164.9 208.2	21.5 18.1 14.8 14.6	211.8
Sierra de San Luis	APM 39-08	-66.11933 -32.76417	1745	61.172 53.190 81.004	1.6 1.6 1.6	2.62 2.08 3.30	1.8 1.8 1.8	0.885 1.123 1.629	2.4 2.4 2.4	0.34 0.54 0.49	918.0 0.0 538.9	0.386 0.349 0.294	5 5 5	0.73 0.77 0.78	176.0 185.1 179.4	241.7 238.9 231.3	22.6 19.4 18.8	237.3
San Francisco del Monte de Oro	APM 40-08	-66.16617 -32.73950	1775	55.491 132.291 54.942 46.785	1.6 1.6 1.6 1.6	1.92 4.19 1.88 1.63	1.8 1.8 1.8 1.8	1.013 1.971 0.815 0.731	2.4 2.4 2.4 2.4	0.53 0.47 0.43 0.45	407.0 497.7 449.6 445.9	0.113 0.725 0.170 0.090	8 7 7 8	0.79 0.81 0.78 0.75	209.5 230.4 215.8 210.5	266.8 283.1 277.5 281.5	21.0 20.4 22.4 24.9	277.2
	APM 45-08 (migmatite)	-66.15600 -32.66633	966	172.097 492.653 289.397 192.049 322.685	1.6 1.6 1.6 1.6 1.6	5.87 13.84 7.34 6.77 9.06	1.8 1.8 1.8 1.8 1.8	0.829 4.443 3.359 1.498 2.902	2.4 2.4 2.4 2.4 2.4	0.14 0.32 0.46 0.22 0.32	631.4 836.0 456.0 486.0 649.3	0.263 1.211 0.781 0.278 1.425	5 5 5 5 6	0.82 0.83 0.84 0.84 0.85	230.2 267.6 287.3 218.9 267.6	280.9 320.9 343.9 260.0 315.5	20.1 21.8 23.1 17.3 20.4	304.2
	APM 46-08 (granitoid)	-66.17167 -32.68650	1008	88.295 307.452 558.316	1.6 1.6 1.6	3.75 7.88 25.90	1.8 1.8 1.8	1.336 3.498 9.674	2.4 2.4 2.4	0.36 0.44 0.37	239.4 930.0 930.0	1.030 4.385 4.385	6 6 6	0.83 0.87 0.89	177.1 285.2 161.6	213.4 326.3 182.1	14.6 19.3 10.4	240.6
	APM 47-08 (migmatite)	-66.18900 -32.70400	1077	81.732 196.059 50.975	1.6 1.6 1.6	2.69 7.00 2.08	1.8 1.8 1.8	0.771 1.325 1.641	2.4 2.4 2.4	0.29 0.19 0.79	391.4 586.7 347.7	0.222 0.501 0.428	5 5 5	0.84 0.84 0.82	230.9 217.7 168.4	275.8 260.6 205.2	18.5 17.7 14.3	247.2
Sierra de El Gigante	APM 51-08 (schist)	-66.92200 -32.86667	638	85.106 25.001 18.856	1.6 1.6 1.6	3.323 0.817 0.576	1.8 1.8 1.8	0.658 0.257 0.219	2.4 2.4 2.4	0.20 0.31 0.38	560.7 227.3 191.2	0.242 0.020 0.068	5 21 22	0.79 0.76 0.75	199.0 231.3 243.6	250.6 304.4 324.0	19.4 26.1 28.4	292.9
Sierra de Pocho Los Tuneles	APM 55-08 (granitoid)	-65.37667 -31.37400	1177	22.789 52.236 95.552 41.810 29.961	1.6 1.6 1.6 1.6 1.6	0.826 1.791 2.653 1.319 1.026	1.8 1.8 1.8 1.8 1.8	0.221 0.244 0.232 0.062 0.123	2.4 2.4 2.4 2.4 2.4	0.27 0.14 0.09 0.05 0.12	255.3 174.9 195.7 259.9 312.8	0.108 0.042 0.021 0.022 0.036	9 9 10 10 10	0.74 0.79 0.83 0.80 0.76	210.9 229.3 284.9 253.8 230.4	283.9 289.3 344.0 318.9 302.3	25.6 22.6 24.1 24.7 25.9	307.7
	APM 59-08 (phyllite)	-65.42600 -31.35883	527	84.593 63.232	1.6 1.6	2.338 2.150	1.8 1.8	1.296 0.835	2.4 2.4	0.55 0.39	144.9 160.3	0.112 0.130	5 6	0.86 0.84	259.1 218.9	302.4 259.1	18.9 16.9	280.8
Sierra de Valle Fértil	APM 12-09 (gneiss)	-67.54256 -30.56240	908	442.594 139.404 371.670 138.088	1.6 1.6 1.6 1.6	11.09 3.82 9.18 3.48	1.8 1.8 1.8 1.8	4.300 1.546 3.340 1.626	2.4 2.4 2.4 2.4	0.39 0.40 0.36 0.47	351.2 266.3 486.8 268.6	0.466 0.142 0.327 0.082	10 10 11 11	0.88 0.84 0.86 0.85	295.0 269.5 300.6 288.5	334.2 322.3 348.7 340.9	19.3 21.6 21.6 22.1	336.5
	APM 15-09 (granitoid)	-67.49066 -30.63729	882	1132.818 412.561 229.753 272.565	1.6 1.6 1.6 1.6	24.17 10.63 5.52 6.66	1.8 1.8 1.8 1.8	14.847 5.372 2.433 3.543	2.4 2.4 2.4 2.4	0.61 0.51 0.44 0.53	517.3 673.2 491.2 474.4	0.452 2.932 0.130 0.169	14 14 8 8	0.89 0.84 0.84 0.85	329.6 279.9 304.3 293.7	369.2 331.4 364.3 346.3	20.4 21.6 24.5 22.3	352.8
	APM 16-09 (amphibolite)	-67.36539 -31.44892	636	142.101 138.499 24.655 42.817	1.6 1.6 1.6 1.6	4.98 4.74 0.81 1.88	1.8 1.8 1.8 1.8	2.891 2.367 0.469 0.900	2.4 2.4 2.4 2.4	0.58 0.50 0.58 0.48	500.7 335.2 505.9 219.3	0.047 0.064 0.003 0.027	9 9 15 10	0.83 0.82 0.83 0.81	204.4 212.4 218.0 167.0	247.3 259.4 264.0 207.4	17.1 18.4 18.2 15.4	244.5

(continued on next page)

Table 1 (continued)

Location	Sample ID (Lithology)	Coordinates [DD.dd]	Altitude [m]	He [ncc]	s.e. [%]	U238 mass [ng]	s.e. [%]	Th232 mass [ng]	s.e. [%]	Th/U	eU [ppm]	Sm mass [ng]	s.e. [%]	Used Ft-corr.	Uncorr. age [Ma]	Ft-corr. age [Ma]	2s [Ma]	Mean age [Ma]	
Cantera Green	APM 20-09 (granitoid)	-65.45101 -35.09387	369	628.190 246.579 403.830 293.964	1.6 1.6 1.6 1.6	27.28 19.76 24.36 12.99	1.8 1.8 1.8 1.8	0.854 0.177 1.121 0.227	2.4 2.4 2.4 2.4	0.03 0.01 0.05 0.02	6889.3 6594.1 8175.4 3466.8	0.161 0.163 0.336 0.211	9 9 9 9	0.76 0.63 0.78 0.80	186.2 102.3 134.2 183.7	244.0 161.7 172.8 230.2	20.9 19.4 14.2 17.8	202.2	
Conlara valley	AUY 27-10 (granitoid)	-65.37598 -33.13835	1171	80.868 94.625	1.6 1.6	2.232 3.142	1.8 1.8	0.463 0.178	2.4 2.4	0.21 0.06	181.4 152.8	0.012 0.038	12 10	0.84 0.86	279.1 240.9	333.4 280.2	22.5 17.8	306.8	
	AUY 29-10 (migmatite)	-65.16814 -32.92813	904	18.994	1.7	0.700	1.8	0.235	2.4	0.34	256.1	0.012	12	0.74	204.4	275.7	24.9	275.7	
	AUY 30-10 (granitoid)	-65.21731 -32.81117	810	15.594 230.192	1.66 1.64	0.403 8.802	1.88 1.81	1.796 3.868	2.41 2.41	4.45 0.44	29.8 349.7	2.59 0.82	9.68 9.70	0.86 0.87	150.5 192.9	175.6 221.8	10.9 13.3	205.8	
Sierra de Pocho Los Tuleles	AUY 38-10 (phyllite)	-65.43324 -31.35132	465	123.488 223.804	1.64 1.64	4.106 6.268	1.81 1.81	1.565 1.392	2.41 2.41	0.38 0.22	552.6 532.9	0.12 0.21	9.87 10.52	0.80 0.82	224.1 274.2	279.7 334.9	21.1 24.0	302.4	
				33.163	1.65	0.863	1.81	0.218	2.41	0.25	189.1	0.02	22.92	1.00	292.7	292.7	13.7		
Sierra de Córdoba Faldas del Carmen	AUY 49-10 (gneiss)	-64.50304 -31.59147	538	40.918 32.739	1.64 1.64	1.408 1.071	1.81 1.81	0.908 0.393	2.41 2.41	0.64 0.37	175.8 139.4	0.01 0.02	8.92 9.24	0.80 0.81	205.3 228.4	257.3 282.7	19.4 20.9	234.3	
				7.283	1.69	0.411	1.84	0.140	2.42	0.34	40.8	0.02	8.28	0.82	134.3	162.9	11.5		
<i>Apatite</i>																			
Santa Rosa de Calamuchita	APM 02-08 (migmatite)	-64.63000 -32.08067	805	7.910 1.200	1.67 1.91	0.53 0.08	1.82 1.97	0.010 0.000	3.75 186.61	0.02 0.00	187.1 38.4	1.11 0.57	2.10 2.28	0.83 0.85	119.4 115.1	144.3 135.0	10.2 9.3	139.7	
Conlara valley	APM 20-08	-65.276500	631	2.716	1.73	0.12	1.89	0.01	3.42	0.08	30.8	0.54	2.07	0.91	179.21	197.00	10.99	180.3	
Santa Rosa de Conlara		-32.310166		1.881 1.319	1.78 1.85	0.10 0.06	1.91 2.12	0.01 0.01	3.87 4.15	0.06 0.09	14.6 18.2	1.01 0.42	1.94 1.98	0.93 0.93	139.70 179.45	150.47 193.31	8.05 11.02		
	APM 28-08 (gneiss)	-66.54650 -34.03100	548	0.445 0.328	1.88 2.00	0.038 0.028	2.57 2.93	0.003 0.006	8.36 5.79	0.09 0.20	8.3 11.1	1.12 0.64	5.00 5.23	0.80 0.80	76.9 78.1	96.6 97.8	8.1 8.5	97.2	
Sierra de Varela	APM 39-08 (granitoid)	-66.11933 -32.76417	1745	0.985 0.930	1.73 1.74	0.04 0.04	2.12 2.19	0.018 0.018	2.84 2.86	0.43 0.46	13.4 13.3	0.45 0.43	15.26 16.30	0.82 0.83	160.0 164.6	194.2 198.5	14.7 15.0	196.3	
Sierra de San Luis	APM 40-08 (granitoid)	-66.16617 -32.73950	1775	0.389 0.224	2.33 2.72	0.03 0.02	3.78 3.91	0.009 0.004	3.57 4.42	0.35 0.16	2.5 4.9	0.38 0.20	11.27 12.26	0.93 0.84	99.8 70.9	106.9 84.8	8.8 8.6	95.9	
San Francisco del Monte de Oro	APM 45-08 (migmatite)	-66.15600 -32.66633	966	0.575 4.936	1.79 1.66	0.10 0.39	1.89 1.82	0.012 0.009	3.16 3.47	0.12 0.02	42.0 51.0	0.18 0.65	12.26 12.82	0.80 0.85	47.2 102.4	59.0 120.7	4.6 8.0	169.6	
				5.239 12.296	1.65 1.64	0.19 0.53	1.83 1.81	0.008 0.015	3.51 2.94	0.04 0.03	60.4 56.7	0.48 1.33	12.12 12.06	0.81 0.80	217.2 184.0	267.7 231.2	19.8 17.9		
	APM 46-08 (granitoid)	-66.17167 -32.68650	1008	1.920 5.587	1.68 1.65	0.12 0.36	1.86 1.82	0.015 0.010	2.97 3.36	0.12 0.03	23.2 57.7	0.31 0.20	17.48 18.20	0.89 0.83	120.4 124.5	135.5 150.3	8.0 10.6	142.9	
	APM 47-08 (migmatite)	-66.18900 -32.70400	1077	3.432 2.022	1.67 1.69	0.12 0.07	1.86 1.94	0.012 0.009	3.19 3.46	0.09 0.12	18.9 15.2	1.14 0.73	48.61 52.16	0.88 0.83	206.7 199.0	234.3 240.8	21.0 25.0	237.5	
	APM 51-08 (schist)	-66.92200 -32.86667	638	0.012 0.015	6.06 5.85	0.005 0.005	13.78 12.57	0.003 0.003	9.92 8.67	0.51 0.62	1.7 1.4	0.05 0.04	5.08 5.22	0.83 0.87	16.8 20.5	20.2 23.6	5.2 5.5	21.9	
Sierra de El Gigante	APM 55-08 (granitoid)	-65.37667 -31.37400	1177	20.476 4.364	1.64 1.66	0.84 0.19	1.81 1.83	0.011 0.012	3.21 3.16	0.06 0.06	129.8 71.1	1.09 0.27	23.74 24.72	0.88 0.86	196.52 179.67	224.11 209.84	13.54 13.55	216.9	
Sierra de Pocho	APM 59-08	-65.42600	527	0.895	1.73	0.02	3.02	0.210	2.44	10.72	2.9	0.36	12.07	0.72	101.91	142.29	14.17	159.9	
Los Tuleles		-31.35883		1.092	1.71	0.06	2.01	0.045	2.56	0.79	47.7	0.09	12.14	0.74	130.63	177.63	16.45		
Sierra de El Gigante	APM 02-09 (schist)	-66.83339 -32.89684	689	0.061 0.077	2.87 2.46	0.01 0.01	11.56 11.59	0.009 0.011	3.16 2.90	1.09 1.40	1 1.4	0.12 0.16	5.61 5.45	0.84 0.84	44.4 55.1	52.8 65.4	9.4 10.7	59.1	
	APM 04-09 (schist)	-66.87234 -32.86408	692	0.042 0.000	3.46 4.14	0.01 0.01	11.48 9.44	0.013 0.014	3.08 3.00	2.76 2.54	1.7 1.7	0.05 0.08	32.53 35.11	0.85 0.79	42.5 32.2	50.3 40.8	7.9 6.4	45.5	
Sierra de Valle Fértil	APM 12-09 (gneiss)	-67.54256 -30.56240	908	0.437 0.256	1.85 2.07	0.12 0.06	1.87 2.07	0.031 0.019	2.48 2.58	0.26 0.31	83.3 28.6	0.57 0.37	3.51 3.45	0.45 0.47	27.5 30.4	61.1 64.8	10.5 10.9	62.9	
	APM 15-09 (granitoid)	-67.49066 -30.63729	882	1.543 3.226	1.70 1.67	0.07 0.13	2.04 1.87	0.081 0.143	2.42 2.41	1.12 1.06	49.8 47.6	0.23 0.36	2.89 3.23	0.46 0.49	135.9 154.1	296.7 313.8	50.2 49.9	293.5	
				2.857	1.67	0.11	1.90	0.130	2.41	1.22	44	0.39	2.90	0.62	166.3	270.0	33.4		
				636	0.103	2.34	0.11	1.91	0.268	2.41	2.40	18.4	1.54	3.58	0.73	4.5	6.2	0.6	5.1

Cantera Green	APM 16-09 (amphibolite)	-67.36539 -31.44892	0.052 0.019	3.00 4.55	0.07 0.03	2.05	0.135	2.41	1.83	24	0.60	5.04	0.88	3.9	4.4	0.3		
Conlara valley	APM 20-09 (gneiss)	-65.45101 -35.09387	369	3.750 1.172	1.66 1.72	0.20 0.07	1.83 1.96	0.014 0.009	2.99 3.43	0.07 0.13	49.1 40.2	0.29 0.07	25.69 26.78	0.85 0.75	146.5 137.8	172.1 183.7	11.3 16.6	
	AUY 27-10 (granitoid)	-65.37598 -33.13835	1171	0.832 0.683	2.07 2.12	0.043 0.042	2.34 2.36	0.002 0.001	5.77 12.86	0.05 0.02	8 7.1	0.74 0.74	5.25 5.21	0.89 0.89	136.7 117.3	154.3 131.4	10.4 8.9	
	AUY 28-10 (granitoid)	-65.13318 -32.94683	922	0.391 2.360	2.54 1.80	0.021 0.136	3.64 1.88	0.004 0.011	4.82 3.36	0.19 0.08	3.9 37.9	0.19 0.10	5.50 5.84	0.91 0.86	138.2 138.9	151.1 161.3	12.8 10.6	
	AUY 29-10 (migmatite)	-65.16814 -32.92813	904	0.483 0.792	2.38 2.08	0.047 0.081	2.26 1.99	0.006 0.003	4.10 5.31	0.13 0.04	22.8 33.4	0.30 0.46	5.56 5.62	0.82 0.81	77.9 76.7	94.4 94.3	7.7 7.4	
	AUY 30-10 (granitoid)	-65.21731 -32.81117	810	2.543 0.408	1.78 2.44	0.185 0.032	1.85 2.75	0.042 0.009	2.60 3.57	0.23 0.28	16.9 13.5	0.66 0.66	5.46 5.42	0.89 0.80	93.5 85.4	104.9 107.0	6.1 9.7	
	AUY 33-10 (pegmatite)	-65.30370 -32.52856	705	0.054 0.090	5.34 4.39	0.005 0.005	15.35 15.18	0.005 0.005	4.44 4.25	0.98 1.13	1.3 1.4	0.20 0.42	5.72 5.54	0.90 0.86	59.0 78.2	65.3 90.5	14.4 16.3	
Sierra de Pocho	AUY 38-10 (phyllite)	-65.43324 -31.35132	465	0.458 1.232	2.16 1.89	0.018 0.051	3.98 2.24	0.112 0.162	2.47 2.45	6.21 3.19	23.6 43.2	0.06 0.61	6.61 5.72	0.82 0.86	84.1 94.1	102.1 109.0	8.2 6.7	
Los Tuneles								2.724	1.74	0.193	1.85	0.176	2.45	0.91	101.6	4.4	5.62 5.72	0.86 0.87
Sierra de Córdoba	AUY 49-10 (gneiss)	-64.50304 -31.59147	538	0.142 0.275	2.79 2.31	0.014 0.039	4.91 2.39	0.005 0.008	4.27 3.61	0.34 0.20	5.4 11.6	0.60 0.23	2.20 2.35	0.86 0.89	59.8 53.3	69.6 59.9	6.7 4.2	
Falda del Carmen				0.027 0.059	6.00 4.23	0.005 0.009	11.12	0.002	5.38	0.45	8.7	0.12	2.61	0.79	31.7	39.9	8.6	
								7.13	0.003	4.84	0.37	7.4	0.13	2.45	0.81	46.7	57.8	8.8

Notes: DD.dd = Latitude and Longitude in decimal degree, uncorr. = uncorrected age, and Ft-corr. = Ft-corrected age. Amount of He is given in nano-cubic-cm in standard temperature and pressure; amount of radioactive elements are given in nanograms; ejection correct. (Ft): correction factor for alpha-ejection (according to Farley and Wolff (1996) and Hourigan et al. (2005)); uncertainties of He and the radioactive element contents are given as 1 sigma, in relative error %; uncertainty of the single grain age is given as 2 sigma in Ma and it includes both the analytical uncertainty and the estimated uncertainty of the Ft; uncertainty of the sample average age is 2 standard error, as $(SD)/(n)^{1/2}$; where SD = standard deviation of the age replicates and n = number of age determinations. Four to six aliquots per sample were picked and analysed. If the investigated age of a single grain deviates by more than 2σ from the mean age, the aliquot was rejected. These erroneous ages can be caused by several factors, such as zoning of alpha-emitting elements, micro inclusions, the limit of detection, or the bias of the ejection correction (smaller grains have larger errors).

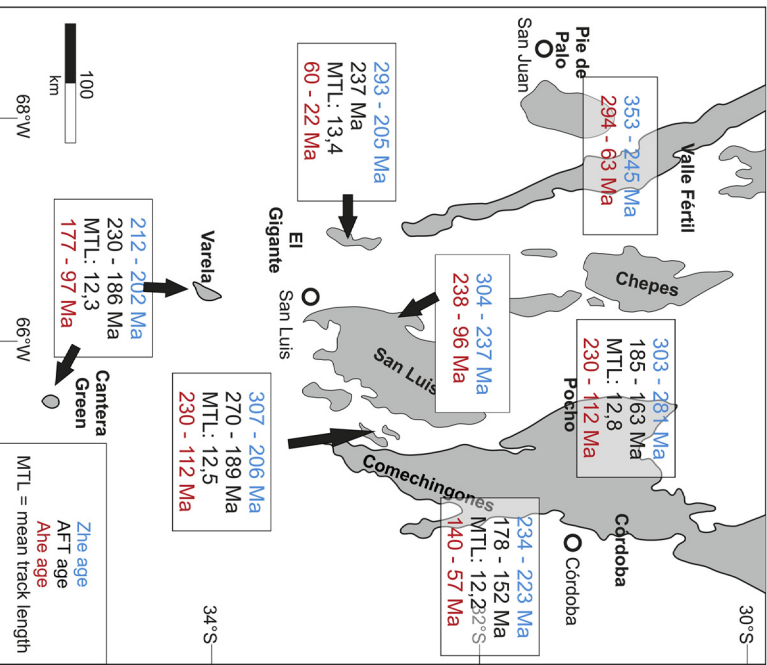


Fig. 4. Compiled map of low-temperature thermochronological data for the Sierras Pampeanas presented in this study.

2. Methodology

Utilizing a combination of several thermochronometers, i.e. apatite fission-track (AFT) and (U-Th)/He dating of zircon and apatite (ZHe and AHe, respectively), is an effective approach to reconstructing the thermal history of the upper crust below 200 °C, which is equivalent to a depth of approximately 10–8 km, assuming a geothermal gradient between 20° and 26 °C/km (e.g. Farley and Wolff, 1996). The temperature interval of the AFT system is sensitive for the so-called "partial annealing zone" (PAZ, e.g. Gleadow and Fitzgerald, 1987), which ranges from 110 °C to 60 °C for typical apatite affected by moderate cooling rates (e.g. Ketcham et al., 1999; Laslett et al., 1987). The comparable temperature range for the (U-Th)/He systems, the "partial retention zone" (PRZ, e.g. Baldwin and Lister, 1998; Wolf et al., 1998), is 200–160 °C for zircon (PRZ_Z) and 80–55 °C for apatite (PRZ_A; Farley, 2000; Reiners et al., 2004). Since these temperature intervals strongly depend on the retentivity of radiogenic He and fission-tracks in the zircon and apatite crystals, the grain size, crystal morphology, effective uranium content, and cooling rate, retention behaviour directly affects these temperature ranges (e.g. Ehlers and Farley, 2003; Reiners and Brandon, 2006; Wolf et al., 1996). For the AFT, the kinetic parameter, usually expressed by the chlorine content or by the etch-pit diameter (D_{par}) of fission-tracks, controls the retention behaviour (Donelick et al., 1999; Ketcham et al., 1999).

In this study, basement samples from the Sierra de Pocho, the Conlara Valley (including the Sierra del Morro), the Sierras de Córdoba, the Sierra del Gigante, the Sierra de Varela, Cantera Green, the Sierra de Valle Fértil, and the Sierra de la Huerta (Fig. 1) were analysed using the ZHe and AHe dating systems. Corresponding apatite fission-track data was obtained from samples from the Sierra de Pocho, the Conlara Valley, the Sierra

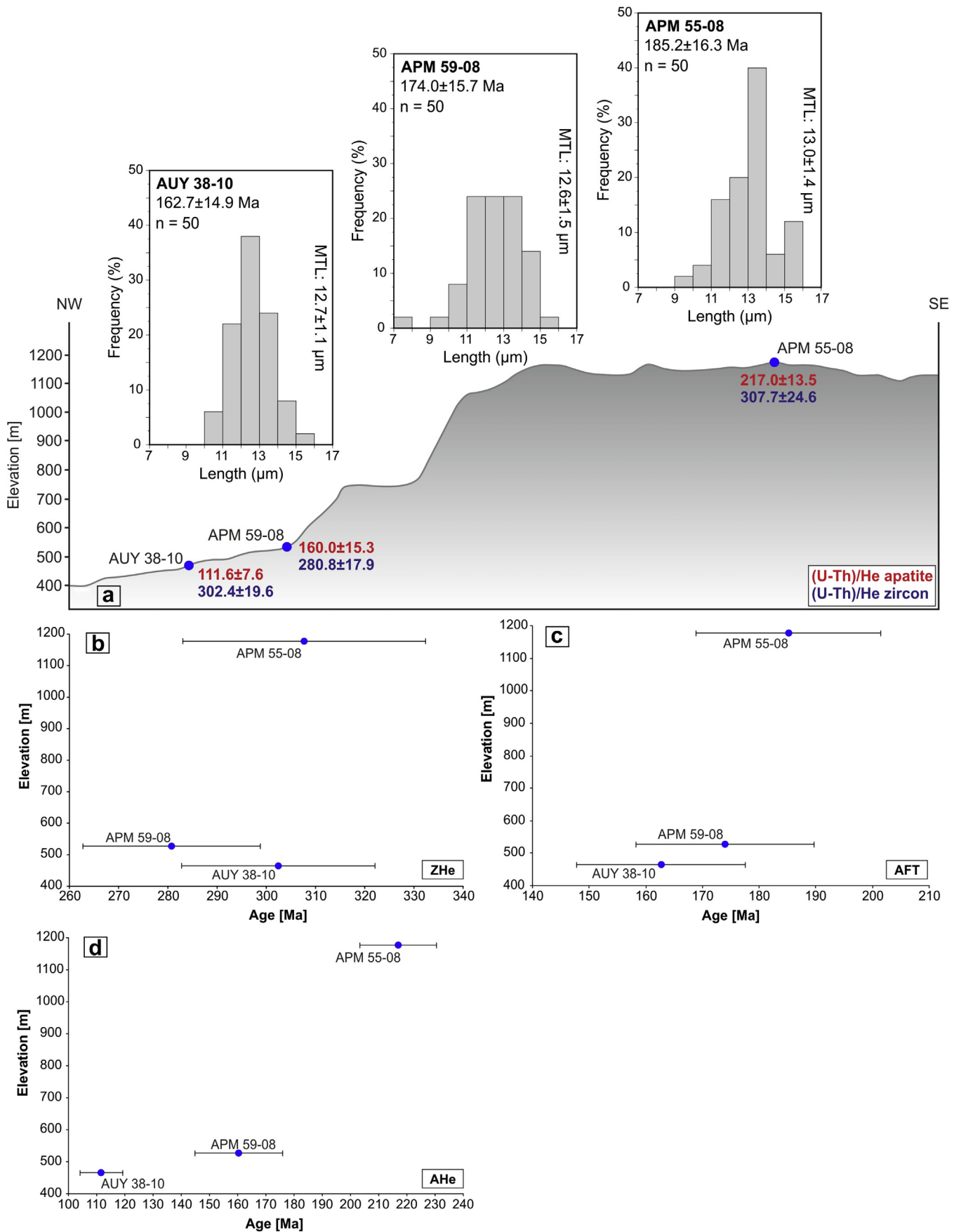


Fig. 5. Thermochronological ages of samples from the Sierra de Pocho a) Schematic profile across the Sierra de Pocho with sample locations, ZHe, AFT, AHe ages as well as AFT length distribution, n = number of confined tracks measured, MTL = mean track lengths are shown; b-d) age–elevation plots for the ZHe, AFT and AHe systems.

Table 2
Apatite fission-track data.

Sample	Longitude (W)	Latitude (S)	Elevation [m]	n	ρ_s	N_s	ρ_i	N_i	ρ_d	N_d	$P(X^2)$ [%]	Age [Ma]	$\pm 1\sigma$ [Ma]	MTL [μm]	s.d. [μm]	Dpar [μm]	s.d. [μm]
APM 20-09	65°27'04"	35°05'38"	369	25	21.19	1429	12.06	813	6.54	6342	41.9	185.6	17.4	12.2	1.4	1.7	0.09
AUY 49-10	64°30'11"	31°35'29"	538	25	9.01	438	5.21	253	6.45	5725	100.0	177.9	19.9	12.4	1.8	1.9	0.15
APM 51-08	66°55'19"	32°52'00"	638	25	1.97	226	1.04	119	7.85	7368	100.0	236.5	32.7	13.4	1.2	2.0	0.11
AUY 28-10	65°07'59"	32°56'49"	922	25	18.51	1669	9.39	847	6.00	5725	32.3	188.8	17.1	12.4	1.7	1.9	0.09
AUY 29-10	65°10'05"	32°55'41"	904	25	24.53	2058	14.40	1208	7.43	5725	66.2	201.4	17.6	12.6	1.7	1.9	0.10
AUY 30-10	65°13'02"	32°48'40"	810	25	18.33	2026	9.64	1066	6.25	5409	47.1	189.2	16.7	12.8	1.6	1.8	0.09
AUY 33-10	65°18'13"	32°31'43"	705	25	10.85	691	4.68	298	6.75	5409	9.4	269.9	32.5	12.2	1.5	1.8	0.11
AUY 27-10	65°22'34"	33°08'18"	1171	25	15.72	1562	7.70	765	6.71	5725	8.2	223.2	21.3	12.6	1.6	1.9	0.10
APM 02-08	64°37'48"	32°04'50"	805	21	21.66	781	13.42	484	5.91	5725	78.5	152.3	15.0	12.0	1.6	1.9	0.16
APM 55-08	65°22'36"	31°22'26"	1177	25	36.25	2426	19.36	1296	6.21	6086	9.3	185.2	16.3	13.0	1.4	2.1	0.12
APM 59-08	65°25'34"	31°21'32"	527	25	18.26	1951	10.93	1167	6.42	6086	14.1	174.0	15.7	12.6	1.5	2.4	0.27
AUY 38-10	65°26'00"	31°21'05"	465	25	23.41	1413	13.24	799	5.75	5409	56.9	162.7	14.9	12.7	1.1	1.9	0.12
APM 28-08	66°32'47"	34°01'52"	548	25	16.61	1265	8.71	663	7.58	7368	97.8	229.6	21.2	12.5	1.2	2.1	0.13

Notes: n, number of dated apatite crystals; ρ_s/ρ_i , spontaneous/induced track densities ($\times 10^5$ tracks cm^{-2}); N_s/N_i , number of counted spontaneous/induced tracks; N_d , number of tracks counted on dosimeter; $P(X^2)$, probability obtaining chi-squared value (X^2) for n degree of freedom (where n is the number of crystals – 1); age $\pm 1\sigma$ is central age ± 1 standard error Galbraith and Laslett (1993); ages were calculated using zeta calibration method Hurford and Green (1983); glass dosimeter CN-5, and zeta value of SL is 323.16 ± 10.1 ; MTL, mean track length; s.d., standard deviation of track length distribution and Dpar measurements; N, number of tracks measured; Dpar, etch pit diameter.

del Morro, the Sierras de Córdoba, the Sierra del Gigante, the Sierra de Varela, and Cantera Green (Fig. 1). The mineral separation and analytical procedures applied are described in detail by Löbens et al. (2011).

3. Results

3.1. Zircon (U–Th)/He ages

ZHe ages from twenty samples were obtained during this study. Sample locations are shown in Fig. 1; analytical results are displayed in Table 1 and Fig. 4. Ages of samples from the Sierra de Valle Fértil vary between Early Carboniferous (353 Ma; APM 15-09) and Early Triassic (245 Ma; APM 12-09), becoming progressively younger from north to south. Three samples from the Sierra del Gigante yield ages ranging from Early Permian (293 Ma; APM 51-08) in the west to Middle Cretaceous (105 Ma; APM 02-09) in the east (Fig. 4). Samples from the southernmost expressions of the Sierras Pampeanas, i.e. the Sierra de Varela and Cantera Green area, yield Late Triassic ages (212 Ma; APM 28-08 and 202 Ma; APM 20-09). Samples from the Conlara Valley region between the Sierras de San Luis and Comechingones range from the Late Carboniferous (307 Ma; AUY 27-10) to the Late Triassic (206 Ma; AUY 30-10). Samples collected along an elevation profile in Sierra de Pocho (Fig. 5) yield Late Carboniferous (308 Ma; APM 55-08) to Early Permian (281 Ma; APM 59-08) ages (Fig. 4).

The five samples from the San Francisco del Monte de Oro profile yield ages from the Late Carboniferous (304 Ma; APM 45-08) to the Middle Triassic (237 Ma; APM 39-08; Fig. 4). Individual samples from the Sierra de Comechingones (APM 02-08, AUY 49-10) show Middle to Late Triassic ages (223 Ma; APM 2-08 and 234 Ma; AUY 49-10; Fig. 4).

3.2. Apatite fission-track ages

Thirteen basement samples from the Eastern Sierras Pampeanas were dated using the AFT method, i.e. the Sierra de Pocho, the Conlara Valley (including the Sierra del Morro), the Sierras de Córdoba, the Sierra de Varela, the Sierra del Gigante, and Cantera Green, the most southern exposure of the Pampean ranges (Figs. 1, 4–6, Table 2). All investigated samples passed the chi-squared test.

Three samples from the Sierra de Pocho were analysed from a ~700 m elevation profile on the western side of the mountain

range. The central ages range from 185 Ma to 163 Ma, correlating positively with elevation (Fig. 6). Track-length distributions are generally unimodal and moderately reduced with a mean of $12.8 \pm 1.3 \mu\text{m}$ (Fig. 6). Dpar values vary from $1.9 \pm 0.1 \mu\text{m}$ to $2.4 \pm 0.3 \mu\text{m}$ (see also Fig. 4).

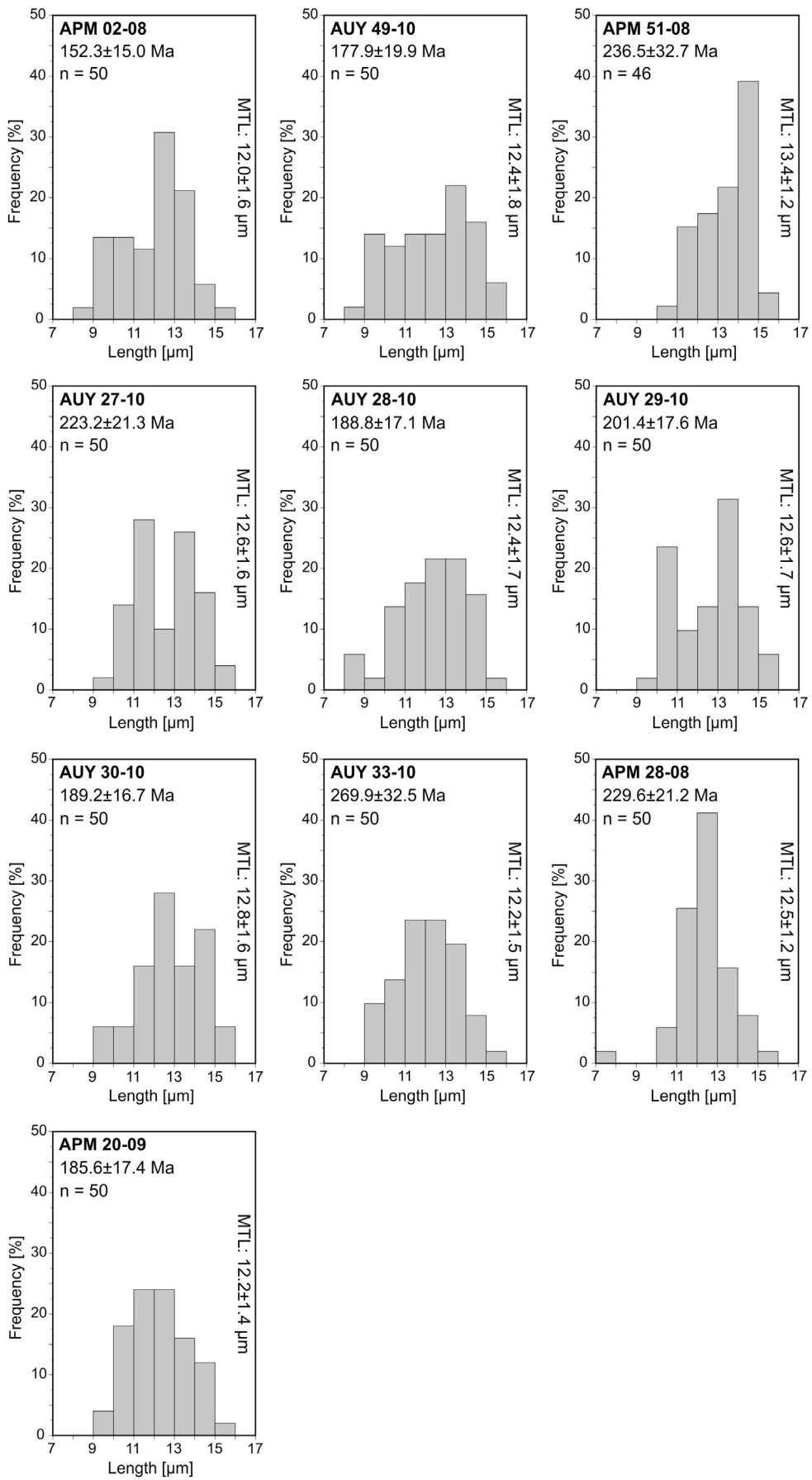
Five basement samples were analysed from the Conlara Valley, including the Sierra del Morro (Figs. 1 and 4). The four samples collected directly from the former (AUY 28-10, 29-10, 30-10, 33-10) yield central ages between 270 Ma and 189 Ma. All these samples are characterized by moderately reduced track lengths with a mean of $12.5 \pm 1.6 \mu\text{m}$. Furthermore, the track lengths are unimodally distributed for AUY 28-10 and AUY 33-10, whereas samples AUY 29-10 and AUY 33-10 show a distinct bimodal track-length distribution (Fig. 7). A bimodal track-length distribution is also characteristic of the moderately reduced track lengths of sample AUY 27-10 from the Sierra del Morro, which has a central age of 223 Ma. Dpar values of all five samples are similar, ranging between $1.8 \pm 0.1 \mu\text{m}$ and $1.9 \pm 0.1 \mu\text{m}$ (Table 2).

The samples from the Sierra de Varela (APM 28-08), south of the Sierra de San Luis, and Cantera Green (APM 20-09) yield central AFT ages of 230 Ma and 186 Ma, respectively (Table 2, Fig. 4). Their track lengths are moderately reduced with a mean of $12.5 \pm 1.2 \mu\text{m}$ and $12.2 \pm 1.4 \mu\text{m}$ and show unimodal distributions (Fig. 7). The Dpar value of APM 28-08 is $2.1 \pm 0.1 \mu\text{m}$, whereas the Dpar of APM 20-09 is distinctly shorter, showing a value of $1.7 \pm 0.1 \mu\text{m}$.

Two samples were analysed from the eastern side of the Sierra de Córdoba (APM 02-08, AUY 49-10, Figs. 1 and 4) and one from the eastern side of the Sierra del Gigante (APM 51-08). The former yields central ages between 178 Ma and 152 Ma. Both are characterized by distinctly shortened track lengths with a mean of $12.2 \pm 1.7 \mu\text{m}$, which are unimodally distributed (Fig. 7). Dpar values of both samples are $1.9 \pm 0.2 \mu\text{m}$. The sample from the Sierra del Gigante has a central AFT age of 237 Ma. The track lengths are moderately reduced with a mean of $13.4 \pm 1.2 \mu\text{m}$ and also show a unimodal distribution (Fig. 7), whereas the Dpar value of $2.0 \pm 0.1 \mu\text{m}$ is slightly increased compared to that of the samples from the Sierras de Córdoba.

3.3. Apatite (U–Th)/He ages

Overall, 24 samples were analysed using the AHe dating method (Figs. 1 and 4, Table 1). In general, the mean AHe age of every sample is younger or coincides with its corresponding fission-track age within the 2σ -error. The average AHe ages of the samples from



the elevation profile in the Sierra de Pocho (Fig. 6) vary between the Middle Triassic (230 Ma; APM 55-08) and the Middle Cretaceous (112 Ma; AUY 38-10). Within this cross-section, there is a distinct age–elevation correlation, although sample APM 55-08 show higher AHe ages (overlap within error) than AFT ages of the same sample (Fig. 6). Four basement samples from small ranges within the Conlara Valley region were analysed, yielding average AHe ages between the Late Jurassic (156 Ma; AUY 28-10) and the Late Cretaceous (78 Ma; AUY 33-10). Two samples were taken from the Sierras de Córdoba, showing Early Cretaceous (140 Ma; APM 02-08, Fig. 4) and Late Paleocene ages (57 Ma; AUY 49-10). Mean AHe ages of basement samples from the Sierra del Gigante show Paleocene (59 Ma; APM 02-09, Fig. 4) to Early Miocene ages (22 Ma; APM 51-08). Three samples from the eastern side of the Sierra de Valle Fértil were dated. AHe ages span from the Early Permian (294 Ma; APM 15-09) to the Cenozoic (63 Ma; APM 12-09 and 5 Ma; APM 16-09) in the Sierra de la Huerta, the southernmost extension of the Valle Fértil range (Fig. 1). The five mean AHe ages of samples from the San Francisco del Monte de Oro area range from the Middle Triassic (238 Ma; APM 47-08) to the Middle Cretaceous (96 Ma; APM 40-08). Samples from the southernmost ranges of the Sierras Pampeanas, i.e. the Sierra de Varela and Cantera Green, show Middle Cretaceous (97 Ma; APM 28-08) and Early Jurassic ages (177 Ma; APM 20-09), respectively.

4. Discussion

4.1. Thermal modelling

The thermal history of 22 samples from the Eastern and Western Sierras Pampeanas was modelled following the approach of Ketcham (2005), utilizing the HeFTy software (Fig. 8). The input data for the modelling of 13 samples were the apatite fission-track single grain ages, track-length distribution, and Dpar data, as well as the corresponding (U–Th)/He ages of zircon and apatite. For nine samples, the models were only based on the zircon and apatite (U–Th)/He data. Two boundary conditions were imposed on each thermal model in order to obtain geologically reasonable cooling histories: *i*) the starting-point of the modelled time–temperature path is given by the zircon (U–Th)/He data (age and the effective closure temperature of approximately 175 °C), and *ii*) the end is confined by the mean annual surface temperature of 17 °C (Müller, 1996). In some cases further constraints were set related to the measured ages of the other thermochronometers used (e.g. K–Ar biotite cooling ages).

Analyses of the time–temperature paths obtained also allow the calculation of cooling rates for the time–temperature range between thermochronometers used. However, any rate calculated here has to be considered as a long-term mean cooling rate based on the average best-fit model path, defined by the temperature boundary conditions of the PRZ_Z, PAZ_A, and PRZ_A.

4.2. Thermal evolution of the basement ranges

Due to the thermal histories obtained, as well as to the distribution of the apparent ages of the individual methods, the area of the Sierras Pampeanas has been divided into two “regions”: an eastern one, including the Sierras de Córdoba, Pocho, and San Luis, as well as a western one, containing the Sierras Pie de Palo, Valle Fértil, El Gigante, Varela, and the Cantera Green area (Fig. 1). For samples and ages belonging to either of this ranges see Fig. 1 and Table 1.

4.2.1. Westernmost and southernmost Sierras Pampeanas

Based on the thermochronological data, we propose the following evolution model for the western region, lasting from the post-orogenic phase of the Famatinian Orogeny to today. In general, moderate-to-rapid cooling from the PRZ_Z into the PRZ_A occurred in the northern part of the western region, i.e. the Sierra Valle Fértil, during the Late Paleozoic (Figs. 7 and 8), which is similar to the Sierra de Pie de Palo and the Sierra de San Luis in the Eastern Sierras Pampeanas. Although cooling based on AFT data is not as good constrained in the Sierra Valle Fértil, because no track-length distributions could be determined from samples, the cooling path obtained for sample APM 15-09 seems to best represent the overall cooling trend. Variations of the other models (APM 12-09 and APM 16-09) are interpreted to be related to documented faults, e.g. ~E–W trending discontinuities, within the mountain range (see Mirré, 1976; Vujovich et al., 1996; Otamendi et al., 2009). Therefore, we suggest that exhumation in the region of the Sierra Valle Fértil is presumably related to erosion of a pronounced relief, which probably developed earlier, maybe during the Famatinian Orogeny. Later, during the Permo-Triassic phase (see above), exhumation intensified, which may be related to tectonically triggered erosion. Further cooling and exhumation below the lower thermal boundary of the PRZ_A occurred during the Triassic (Figs. 7 and 8). This is probably due to erosion during Triassic rifting, as indicated by syn-rift deposits at the western margin of the range (e.g. Ramos et al., 2002). The Triassic is followed by very low exhumation from the Jurassic until the Late Cretaceous. Exhumation to near-surface temperatures commenced in the Paleogene, similar to the exhumation of the Sierra de Pie de Palo, but slightly delayed (Figs. 7 and 8). The Jurassic to Cretaceous period of very low exhumation is presumably related to low erosion rates during a period of tectonic quiescence. However, in both areas, the final exhumation to near-surface temperatures is of Paleogene age and probably associated with the early Andean deformation, characterized by ~E–W compression and tectonically-triggered erosion. Therefore, the general structural evolution of the latter range is similar to that of the Sierra Valle Fértil. The Permo-Triassic exhumation period evidenced by our thermochronological data also indirectly indicate that both mountain ranges are potentially characterized by a positive relief since the Late Paleozoic. Considerable evolutionary differences between both ranges only existed during the middle to late Mesozoic, since there was considerable exhumation in the Sierra de Pie de Palo, but not in the Sierra Valle Fértil (Fig. 8). This could be because the topography of the latter range was less pronounced, i.e. the mountain range was characterized by a lower surface elevation, compared to the Sierra de Pie de Palo. Presumably, a relatively lower elevation could be related to rift-related subsidence of the whole range during the Triassic, or the Sierra de Pie de Palo in the west possibly represented an orographic barrier, causing only slow erosion within the region of the Sierra Valle Fértil during that time. However, final exhumation to near-surface temperatures occurred more or less synchronously, as mentioned above.

In the middle part of the western belt, i.e. the Sierra del Gigante (Fig. 1), the onset of cooling and exhumation from PRZ_Z-to-PAZ_A-related temperatures occurred during Permian and Triassic times (APM 51-08 in Figs. 7 and 8), potentially related to the Permo-Triassic exhumation phase (see above). Presumably, this produced relief, which was affected by erosion afterwards, resulting in further exhumation of our samples (Figs. 7 and 8). Furthermore, this topography was probably nearly eroded by Early to Middle

Fig. 6. AFT age and track length distribution for all analysed samples. AFT data for the Sierra de Pocho is displayed in Fig. 5; *n* = number of confined tracks measured, MTL = mean track length, age = apparent central age.

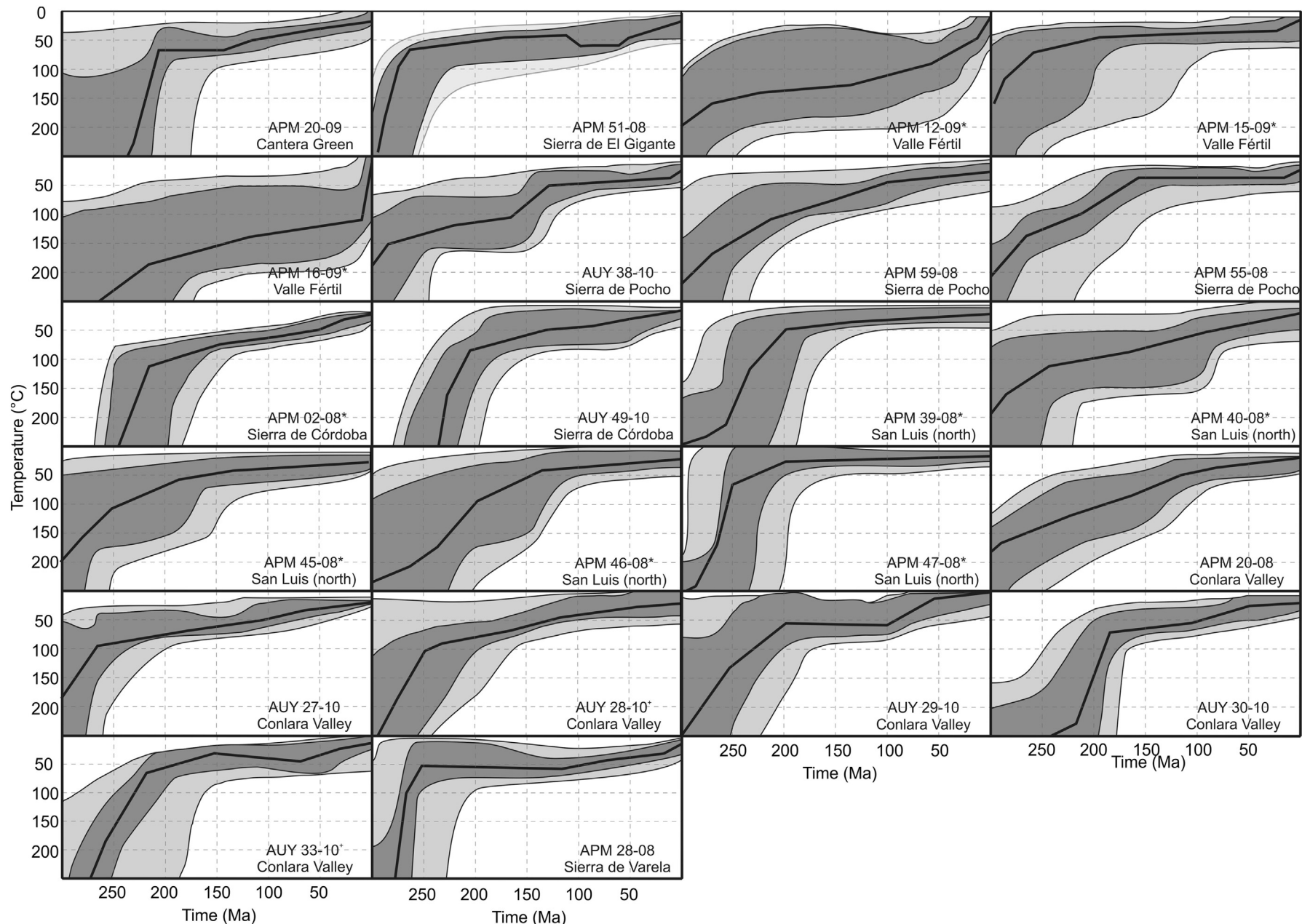


Fig. 7. Results of inverse thermal modelling using HeFTy. Modelled time–temperature paths based on ZHe, AFT and AHe data. The starting-point of modelled paths is constrained by the ZHe age and its respective closure temperature. End of path is constrained by the present day surface temperature. * indicate models without AFT data, + indicate model without ZHe data. Light grey paths: acceptable fit, dark grey: good fit, black line: best fit. For best fit average GOF from AHe, ZHe and AFT age and AFT length distribution is equal or better than 0.6.

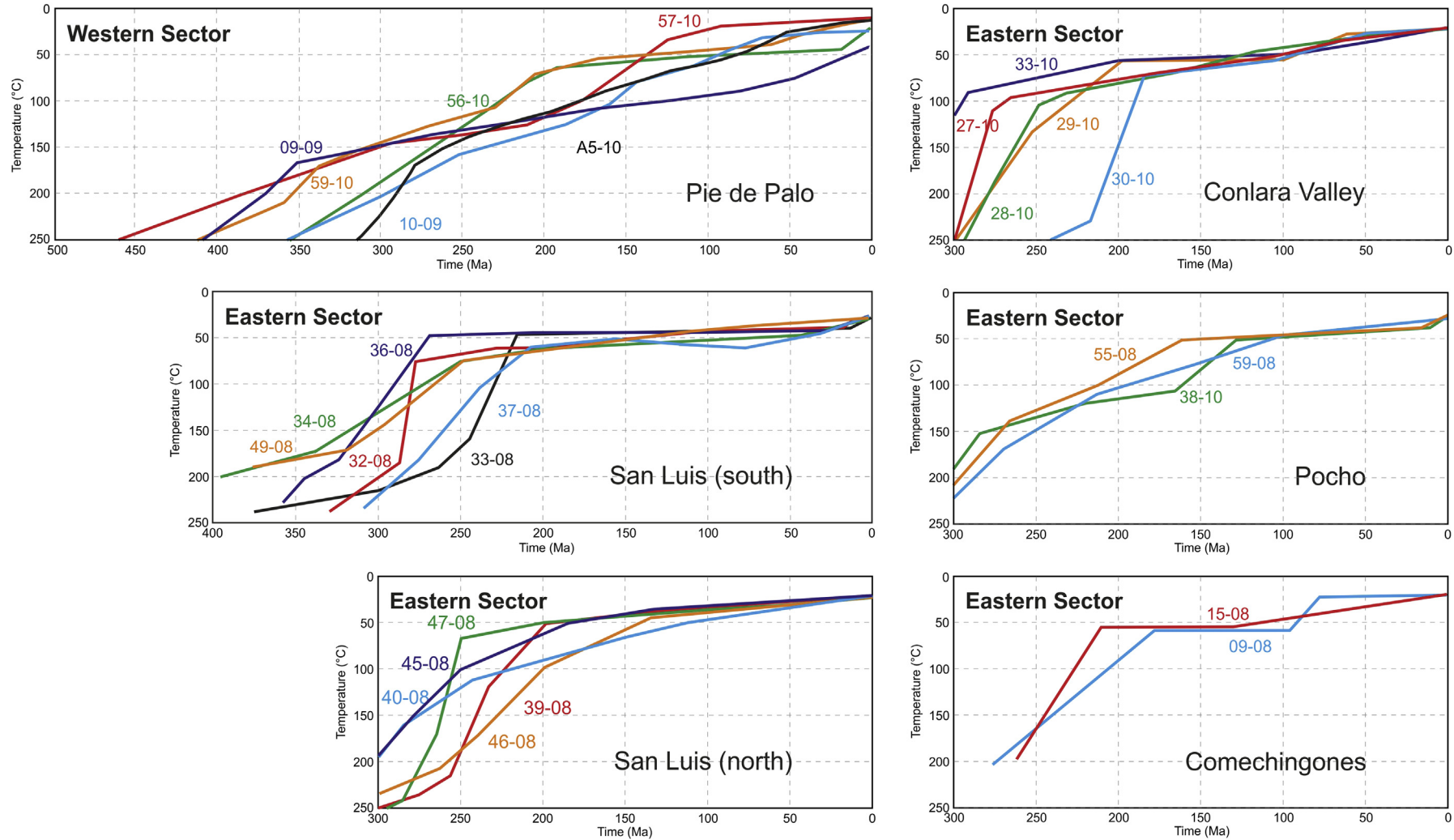


Fig. 8. Comparison of cooling paths from the entire Sierras Pampeanas ordered by region. Displayed paths represent best fitting paths from HeFTy models (see also Fig. 7). Data for the Sierras de Pie de Palo, Comechingones and southern San Luis are taken from (Löbens et al. (2011), Bense (2013) and Löbens (2013). Abbreviated sample ID; -08 is APM, -09 is APM, -10 is AUY. Different colours mark different samples. (For interpretation of the references to colour in this figure legend, the reader is referred to the web version of this article.)

Cretaceous times. Subsequently, Early Cretaceous rifting, linked to the opening of the South Atlantic at these latitudes (e.g. Schmidt et al., 1995; Rossello and Mozetic, 1999), triggered the development of an intracontinental rift basin, i.e. the Beazley Basin (Fig. 9; e.g. Schmidt et al., 1995), in the region of the Sierra del Gigante. Since the latter range is situated within this basin, it is very likely that the observed Cretaceous re-heating of the El Gigante samples (APM 51-08; Figs. 7 and 8) was caused by burial beneath sediments derived from the surrounding heights. The maximum re-heating temperature was around 55 °C, equivalent to a maximum thickness of 2.1–2.8 km (assuming a geothermal gradient of 20–26 °C/km) for the overlying sedimentary succession, which agrees well with the ~2 km of cumulative thickness of the Cretaceous strata in this region (Yrigoyen, 1975). Following this burial, re-exhumation to near-surface temperatures occurred during the Late Paleocene to Neogene (Figs. 7 and 8). Exhumation is potentially related to the Andean deformation, accompanied by erosion stripping off the Cretaceous sediments and leading to exposure of the metamorphic basement. Furthermore, the increasing AHe ages from west to east within this mountain range (Figs. 7 and 8, Table 1) i) indicate Neogene activity of the western main boundary fault as proposed by Schmidt et al. (1995) and ii) suggest a similar thermal evolution as described by Bense (2013) for the Sierra de San Luis.

Within the most southern exposures of the Sierras Pampeanas, i.e. the Sierra de Varela and Cantera Green, rapid cooling from the PRZ_Z into the PRZ_A occurred between Permian and Triassic times (Figs. 1, 7 and 8). This rapid exhumation of both mountain ranges was presumably generated by tectonism accompanied by erosion during the Permo-Triassic compressional phase (see above). Furthermore, the time–temperature histories suggest a younger exhumation of Cantera Green than of the Sierra de Varela (Figs. 7 and 8). Presumably, deformation first affected the western area of the Sierras Pampeanas and propagated towards the east, as also suggested by comparison of the cooling paths from the latter ranges with those from the Sierra Valle Fértil (APM 15-09, 16-09, AUY 38-10, Figs. 7 and 8). Thus, onset of exhumation as well as exhumation into PRZ_A temperatures occurred relatively earlier in the Sierra de Varela because it is located farther in the west than Cantera Green (APM 20-09, Figs. 7 and 8). Samples from the Cantera Green remained within this temperature conditions until the Early Cretaceous (APM 20-09, Figs. 7 and 8), potentially due to tectonic quiescence and very low erosion in this area. The phase of tectonic quiescence is followed by onset of exhumation out of the PRZ_A to near-surface temperatures during the Early Cretaceous (Figs. 7 and 8). Rift-related erosion probably caused this exhumation, which, in turn, is associated with the Atlantic rifting that affected the area at these latitudes during the Cretaceous (e.g. Schmidt et al., 1995). In contrast to Cantera Green, sample from the Sierra de Varela remained within the temperature interval of the PRZ_A until the Late Cretaceous (Figs. 7 and 8). Due to tectonic quiescence in the Cantera Green area, caused by their position offside the Cretaceous rift basins, there was probably very slow erosion, hence very low exhumation in this region during the Jurassic, similar to the area of Cantera Green. However, more or less stagnation within the PRZ_A during the Cretaceous is presumably related to the geographical position of the Sierra de Varela compared to Cantera Green. The latter range was situated beyond the extension of the Cretaceous Beazley Basin (Fig. 9) proposed by Jordan et al. (1989) and Schmidt et al. (1995), whereas the Sierra de Varela was located at the eastern margin of this basin (Fig. 1). Therefore, sediments derived from the surrounding heights were presumably deposited in the vicinity of the Sierra de Varela. However, it is noteworthy that the AHe ages are not reset within this mountain range, in contrast to the Sierra del Gigante (APM 51-08, Figs. 7 and 8). The fact that modelled time–temperature paths do not show Cretaceous burial re-heating

in the Sierra de Varela, can be related to the geographical positions of the range outside the Cretaceous Beazley Basin (Fig. 9). Since the future Sierra del Gigante was located near the inferred rift axis and the main depocenters during the Cretaceous (Schmidt et al., 1995), the Sierra del Gigante area was affected by burial re-heating (as mentioned above), whereas, in the vicinity of the Sierra de Varela, the maximum sedimentary thickness was probably less than 500 m (Jordan et al., 1983), which was insufficient to reset the AHe ages. However, the subsequent cooling and exhumation of the Sierra Varela range during the Late Cretaceous is probably related to cessation of rifting and onset of the slow erosion of Cretaceous sediments in this region. Continuous cooling and exhumation of the Sierras Varela and Cantera Green during the Cenozoic (Figs. 7 and 8) was caused by deformation accompanied by erosion during the Andean Orogeny.

4.2.2. Southeastern Sierras Pampeanas

Thermal modelling of samples from the Nogolí area in the southern Sierra de San Luis show that samples passed through PRZ_Z and PAZ_A temperature conditions during Permian to Middle Triassic times (Figs. 7 and 8). Due to high AHe ages and associated errors, cooling through PRZ_A temperature conditions cannot be exactly constrained by thermal modelling. However, our models indicate a Triassic to Middle Cretaceous age. Subsequent cooling to surface temperatures commenced in post-Permian times, most probably between the Cretaceous and the Paleogene (Fig. 8). From the Sierra de San Luis, cooling rates of <5 °C/Ma for the passage through the PRZ_Z and PAZ_A and <1 °C/Ma for PRZ_A temperature and below are reported (Bense, 2013). Modelled time–temperature paths based on data from the San Francisco del Monte de Oro area (APM 39, 40, 45, 46, 47-08, Fig. 1b) in the northern Sierra de San Luis document cooling through PRZ_Z temperatures in Late Carboniferous to Permian times (Figs. 7 and 8). No AFT data is available, so cooling through PAZ_A temperature conditions is not well constrained. However, cooling through PRZ_A temperatures occurred in Middle Triassic to Cretaceous times (Figs. 7 and 8). Subsequent cooling to surface temperatures is likely to have occurred during Cretaceous time, also it is less constrained by the modelled thermal history. In general, time–temperature conditions from the northern and southern Sierra de San Luis indicate a quite similar thermal history for both regions (Fig. 8).

Several samples were collected from smaller mountain ranges in the Conlara Valley region (AUY 27, 28, 29, 30, 33-10), between the Sierra de San Luis and Sierras de Córdoba (Fig. 1). In general, thermal modelling based on AFT and AHe data shows that PAZ_A temperatures had already been reached in Early Permian times. Passage through PRZ_A temperatures occurred during the Cretaceous. Subsequent cooling to surface temperatures is indicated to have occurred in Cretaceous to Paleogene times.

Modelled time–temperature paths also indicate substantial differences in the thermal history of the area. Samples from the eastern and southern parts of Conlara Valley, i.e. AUY 28-10 and AUY 29-10 as well as AUY 27-10, cooled through PRZ_Z temperatures during Permian times. Subsequent cooling through PRZ_Z and PAZ_A temperatures occurred in Permian to Triassic times, which is very similar to those findings from the Sierra de San Luis (see above); it was followed by decelerated cooling, as suggested by thermal models (Figs. 7 and 8). Cooling through temperatures of the PRZ_A is indicated to have happened synchronously for all Conlara Valley samples during Jurassic to Cretaceous times (Figs. 7 and 8), whereupon surface temperature conditions were probably reached in Late Cretaceous to Paleogene times. Nevertheless, there are minor differences between individual time–temperature paths. Sample AUY 27-10 from the El Morro range in the southern Conlara Valley shows a slightly older thermal history than AUY 28-10 and

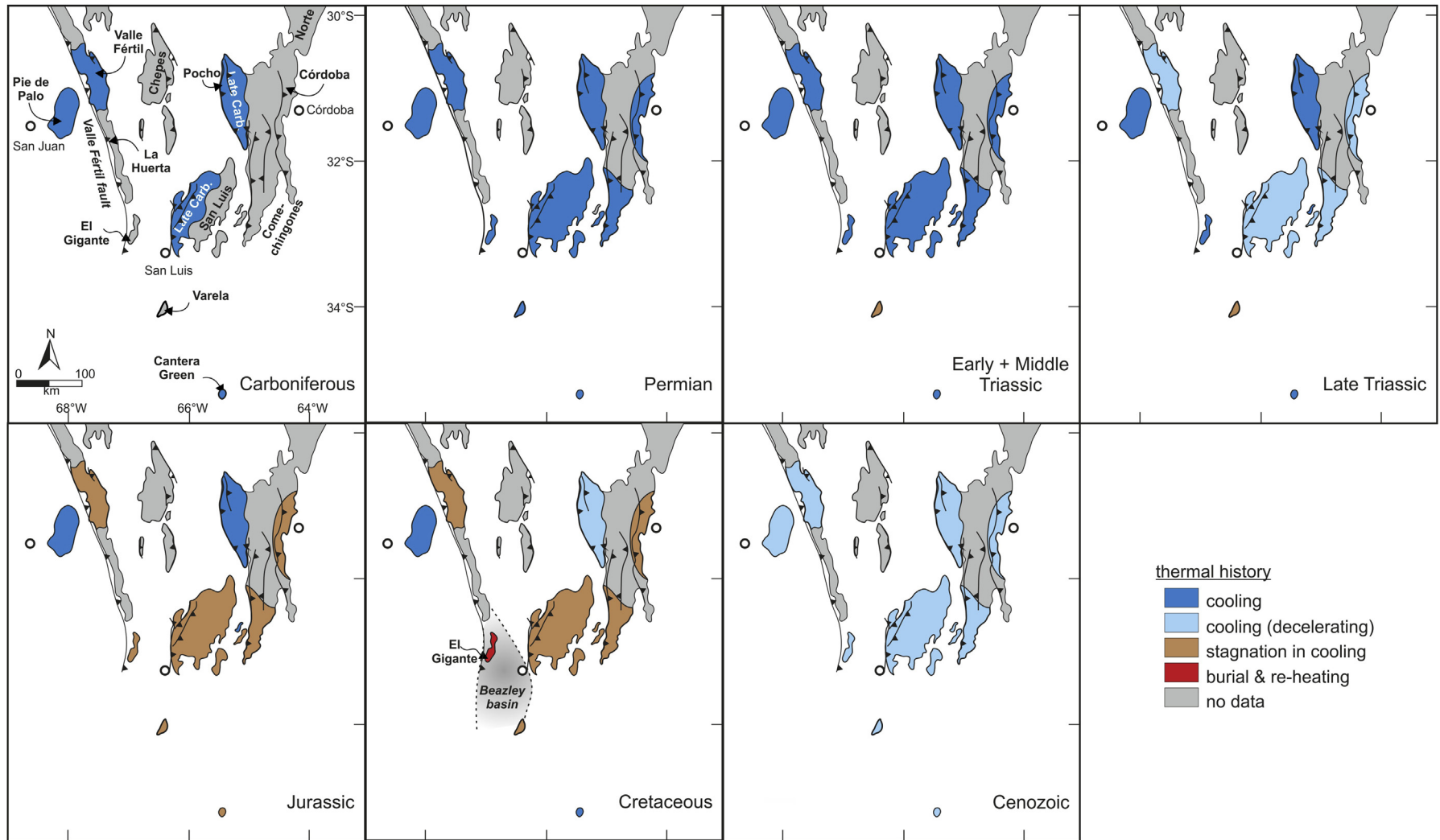


Fig. 9. Schematic map highlighting areas of cooling, stagnation in cooling as well as burial and re-heating within the Sierras Pampeanas from Carboniferous to Cenozoic times, based on thermal modelling. Location of major Paleozoic faults according to González Bonorino (1950) and Jordan and Allmendinger (1986). Further details are discussed in the text.

AUY 29-10. However, one sample (AUY 30-10) shows a significantly younger history than the other samples from the Conlara Valley (Figs. 7 and 8). Instead of Permian PR_Z-cooling ages, AUY 30-10 shows Late Triassic ages. PAZ_A and PR_Z_A temperatures were passed in Jurassic to Cretaceous times. We attribute those differences to an association of the smaller mountain ranges with different basement blocks. El Morro (AUY 27-10) constitutes an individual range, AUY 33-10 belongs to the Sierra de San Luis, and AUY 28-10 and AUY 29-10 are associated with the Sierra de Comechingones. In contrast, AUY 30-10 represents a solitary block within the Conlara Valley with unclear structural affiliation with one of the nearby mountain ranges. Thermal models for the Conlara Valley samples indicate that cooling through the PR_Z_Z and PAZ_A temperature regime coincides with moderate cooling rates between 2.5 and 4.5 °C/Ma, whereas passage through PR_Z_A and post-PR_Z_A temperatures is characterized by slower cooling rates, approximately 0.3–1 °C/Ma.

Time–temperature paths for the Los Tuneles area in the Sierra de Pocho generally show slow cooling. Exhumation through PR_Z_Z temperatures occurred in Permian times. PAZ_A temperatures were passed in Triassic to Jurassic times. Subsequent cooling through the PR_Z_A took place in Late Triassic to Early Cretaceous times. Cooling to surface temperature potentially occurred in Cenozoic times (Figs. 7 and 8).

Modelled time–temperature paths for the Sierra de Pocho suggest cooling rates of around 1–2 °C/Ma for the temperature range between PR_Z_Z and PAZ_A and below 1 °C/Ma for the PR_Z_A temperature range and below.

Samples collected in the western Sierras de Córdoba, between the Sierra de Pocho and the Yacanto area (Fig. 1), indicate Triassic cooling through PR_Z_Z and PAZ_A temperature conditions (APM 39, 40, 45, 46 and 47-08, Figs. 7 and 8). PR_Z_A temperature conditions were passed in Early to Late Cretaceous times, whereby surface temperatures were probably reached in Cretaceous to Cenozoic times (Figs. 7 and 8).

Thermal modelling by Löbens et al. (2011) in the southern Sierra de Comechingones reveals Late Permian ages for cooling through PR_Z_Z temperatures. PAZ_A temperature conditions were reached during Late Triassic to Jurassic times. Cooling from PAZ_A to PR_Z_A temperatures was slow, as indicated by thermal models, reaching PR_Z_A temperatures in Middle Cretaceous times (Fig. 8). Cooling to surface temperatures occurred in Late Cretaceous to Paleogene times (Löbens et al., 2011). The thermal history of the Sierra de Comechingones indicates rates between 1.5 and 4 °C/Ma for cooling through PR_Z_Z and PAZ_A temperatures and <1 °C/Ma for the PR_Z_A and post PR_Z_A temperatures, as reported by Löbens et al. (2011).

The thermal history observed in this part of the Sierras Pampeanas can be linked to several geological and geodynamic processes. The oldest cooling event occurred in the Carboniferous (Figs. 7 and 8). We relate this to the erosion of topography (see Lencinas and Timonieri, 1968) which was built up during previous orogenic phases. Additionally, the Late Carboniferous is characterized by a period of orogenic collapse (Mpodozis and Ramos, 1990), supporting the idea of pronounced cooling during this time period.

As discussed above, the majority of samples passed the PR_Z_Z and PAZ_A in Permian to Triassic times (Fig. 8). This Permo-Triassic time interval is synchronous with an inferred flat-slab subduction episode of the Nazca Plate beneath the South American Plate (Ramos and Folguera, 2009). This event might have led to considerable compression, thus to exhumation and cooling at these latitudes (Bense, 2013). The flat-slab segment was also linked to an orogenic phase in the San Rafael Massif in the province of Mendoza, defined as the San Rafael Orogeny by Kleiman and Japas (2009). Although a direct link between this orogenic phase and the study area has not been developed yet, those findings discussed above

show the importance of this, until now, not well understood Permian to Triassic event for the thermal history of the entire Southern Sierras Pampeanas (see below).

However, further cooling in post-Triassic times is generally characterized by comparatively low cooling rates in the entire Southeastern Sierras Pampeanas. We interpret this to be related to low erosional rates as a consequence of relatively stable tectonic conditions within the sampled mountain ranges without substantial uplift or burial events (see below, Fig. 8). Although the Cenozoic compression that followed may have contributed to the final cooling of samples to temperatures below 50 °C, its influence is not constrained by modelled time–temperature histories.

4.3. Spatial and temporal variability of cooling

Based on the findings discussed above, we conclude that cooling during Permian times in the western regions of the Southern Sierras Pampeanas and its subsequent eastward propagation until Early to Middle Triassic times (Figs. 9 and 10) is spatially and temporally related to a period of flat-slab subduction at these latitudes. This flat-slab subduction event was initially defined for Late Carboniferous to Early Permian times in the Southern Central Andes (Martínez et al., 2006; Ramos et al., 1986), but, based on our data, it also shows a clear imprint in the Southern Sierras Pampeanas. An imprint of this event in the study area is also indicated by a distinct eastward propagation of Late Paleozoic calc-alkaline magmatism from the Southern Central Andes to the Southwestern Sierras Pampeanas (Sierra de Valle Fértil and Sierra de La Huerta, Fig. 1) during Permian to Early Triassic times (see Caminos, 1979; Ramos, 1988; Mpodozis and Ramos, 1990; Mpodozis and Kay, 1990; Varela et al., 1993; Ramos and Folguera, 2009, and references therein). Inversely to its onset, cooling ceased first in the southeastern parts of the region studied and propagated westwards during Late Triassic times (Figs. 8 and 9). Whether or not Triassic rifting along terrane boundaries and crustal unconformities (see Ramos et al., 2002) and subsequent stagnation in cooling is related to the end of flat-slab subduction cannot be solved here.

In contrast, the Sierras de Pie de Palo and Pocho show notably slower but more continuous cooling compared to other modelled time–temperature paths. Additionally, both ranges (in particular, Pie de Palo) show prolongation of cooling, even during periods marked by an extensional tectonic setting (see Figs. 8–10). A possible explanation for this is that both ranges formed topographic heights, subjected by ongoing erosion, unaffected by extensional events causing subsidence and burial. This interpretation as topographic heights is supported by spatial distribution of rift-related sediments in the region studied, showing that none of the Paleozoic faults/suture zones (see above) bounding the Sierra de Pie de Palo and the Sierra de Pocho were significantly extensionally reactivated during Mesozoic rift events (see also Jordan et al., 1983; Schmidt et al., 1995; Ramos et al., 2002). Whether those topographic heights formed by tectonic events or not, cannot be solved here. Additionally, the position of the Sierra de Pie de Palo on the footwall of the Valle Fértil fault presumably did not allow any burial re-heating of the Pie de Palo samples due to rifting along this fault (Fig. 9). Thus, both regions are considered to be relatively unaffected by Late Triassic to Early Jurassic as well as Early Cretaceous rifting.

Another exception is given by sample AUY 30-10 which is in conflict with findings from the surrounding samples. For instance, AUY 30-10 displays accelerated cooling during Late Triassic to Early Jurassic extensional settings. A possible explanation might be related to the complex arrangement of different faults in the Conlara Valley (e.g. Miró and Martos, 1999), leading to some kind of step-over or push-up structure (see van der Pluijm and Marshak,

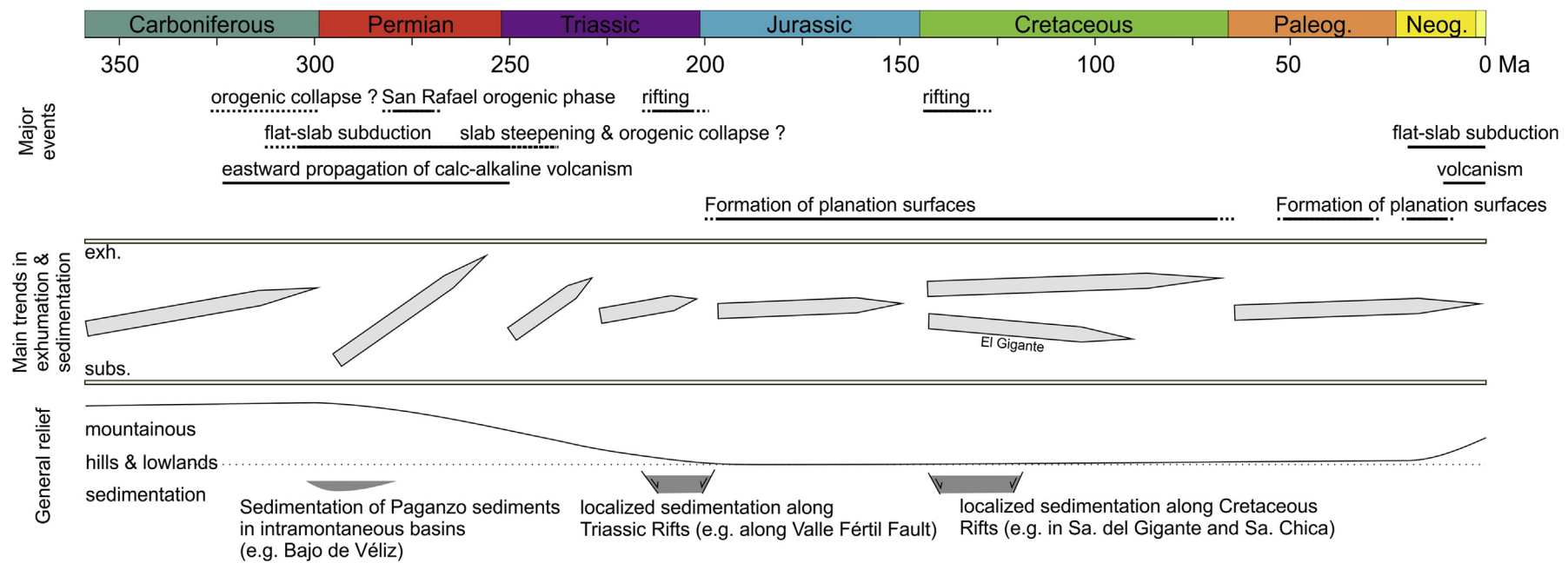


Fig. 10. Summary of the major geological events, sedimentation periods, mean trends in exhumation or subsidence (see also Fig. 9) and the deduced relief evolution of the southern Sierras Pampeanas (see Jordan et al., 1989; Ramos et al., 2002; Schmidt et al., 1995 and references therein for more details). Details are described in the text.

2004). However, since the structural affiliation of this basement block with the surrounding ranges is unclear due to the sedimentary cover of the basement blocks in the Conlara Valley, the thermal history of this minor basement block remains enigmatic.

Finally, thermal modelling indicates that the cooling to near-surface temperatures in the different parts of the Sierras Pampeanas, as far as has been traced by the AHe thermochronometer, occurred between the Latest Cretaceous and the Paleogene (Figs. 8–10).

Part of the Late Cretaceous to Paleogene exhumation, particularly the western parts of the Sierras Pampeanas may seem to constitute the southern continuation of the Eocene exhumation processes that affected vast proportion of the Eastern Cordillera to the north of the study area (see for example Oncken et al., 2006; DeCelles et al., 2007; Hongn et al., 2007). There, the exhumation and associated structuration has been explained by an Eocene flat-slab subduction event affecting the central Altiplano region (James and Sacks, 1999; Kay and Coira, 2009) and the development of the Arica bend/Bolivian Orocline (see Arriagada et al., 2008 for a detailed discussion). However, both events, the Arica bending and the Paleogene flat slab are located far to the north of the study area and it not seems that they have affected the studied region, especially because the Pampean Late Cretaceous to Paleogene exhumation stage shows a higher amplitude, involving almost the whole analysed area. Therefore, this event may not be considered as a simple deformational stage affecting the western border of South America, since it involves exhumation of regions located 500 km east of the Cenozoic trench. Nevertheless, further research is necessary in order to better explain the causes of Late Cretaceous to Paleogene exhumation in the Sierras Pampeanas as well as a potentially linkage to exhumation and deformation events in the Eastern Cordillera.

In a recent review of AFT data from the Sierras Pampeanas, Dávila and Carter (2013) argue that the amount of exhumation and uplift caused by Cenozoic flat-slab subduction was underestimated by recent studies (Jordan et al., 1989; Löbens et al., 2011) because no Cenozoic cooling ages have been found. They argue that this is the result of omitted thermal equilibration of chronological systems due to rapid burial and exhumation of rocks combined with a very low geothermal gradient. Which resulted in a non-reset of thermochronological ages.

However, the argumentation of Dávila and Carter (2013) is only based on AFT data. AFT data alone does not constrain the timing of exhumation to near surface temperatures. Löbens et al. (2011), Bense (2013), Löbens (2013), Bense et al. (2013b) and this study present non-resetted AHe ages, even though the AHe system have a significantly higher temperature sensitivity due to its lower effective closure temperature. Although it is geologically evident that the Neogene flat-slab subduction period led to the uplift of the present-day Sierras Pampeanas (e.g. Ramos et al., 2002), the new thermochronological results discussed here strongly indicate that a positive topography already existed before the Paleogene. Thus, we conclude that previous models (e.g. Ramos et al., 2002) overestimated the amount of uplift and exhumation attributed to flat-slab subduction. Instead, it might be considered that the Andean compression led to an accentuation of a pre-existing relief in the Southern Sierras Pampeanas and that the Neogene influence on exhumation, including the flattening of the subduction angle of the Nazca Plate, has been overestimated so far (see also Löbens et al., 2011 for a more detailed discussion).

4.4. Paleo-surfaces and denudation rates

The Sierras Pampeanas uplifts are defined as a broken foreland during the Andean Orogeny and, at least in their recent structural

configuration, as distinctive surficial characteristics of the Pampean flat-slab segment of the subducting Nazca Plate (Jordan et al., 1983; Jordan and Allmendinger, 1986; Ramos et al., 2002). However, the age and the pre-Andean morphotectonic evolution of those planation surfaces, which are mainly developed on the eastern side of the ranges, have not yet been completely clarified (e.g. Jordan et al., 1983; Carignano, 1999; Rabassa et al., 2010). Since almost no pre-Quaternary sedimentary cover is preserved atop the ranges for constraining the post-Paleozoic relief, the erosional surfaces themselves have to be envisaged as a key geometric marker for this purpose.

Ideas about the geomorphological evolution of the Sierras Pampeanas have already been described and controversially discussed in early works (e.g. Stelzner, 1885; Brackebusch, 1891; Bodenbender, 1890, 1895; 1911; Gross, 1948; González Bonorino, 1950; see also Rabassa et al., 2010 for a recent review). The Evolution has been discussed in two ways.

Gonzalez Diaz (1981) and Criado Roque et al. (1981), based on the ideas of Bodenbender (1905) and Bodenbender (1911), suggested that planation surfaces represent a continuous and essentially synchronous surface, which was uplifted and disrupted during the Andean Orogeny.

Alternatively, Rovereto (1911) first introduced the idea of a diachronous development of the erosional surfaces in the Sierras Pampeanas and considered Paleozoic to Mesozoic ages. The idea of diachronous development was later picked up by other authors (e.g. Jordan et al., 1983; Carignano, 1999), who suggested that topographic scarps between distinct surfaces were the result of juxtaposition of several, individual surfaces with diachronous ages ranging from the Late Paleozoic to the Paleogene.

Although initially not intended to date paleo-land-surfaces or erosional surfaces, recent thermochronological data for the Sierra de Comechingones, Sierra de San Luis, Sierra de Aconquija and Cumbres Calchaquíes, and the Sierra Pie de Palo (see Figs. 7 and 8) support the idea of a diachronous development of erosional surfaces in Jurassic to Cretaceous times.

Especially AHe ages, as well as the calculated denudation rates of the Sierras de San Luis and Comechingones (see above), fit with the suggested formation age of the erosional surfaces proposed by Carignano (1999). However, AHe ages can only be used as an indirect age constraint for erosional surfaces, because exact denudation rates, which led to exhumation of the samples from the PRZA to surface temperatures, are unknown. This is especially important for areas where numerous faults of unknown age are penetrating the basement, as observed in the Southern Sierras Pampeanas (e.g. Simpson et al., 2001; Bense et al., 2013b).

Thermochronological data presented in this study (Figs. 7 and 8), as well as data published by Löbens et al. (2011), indicate slow denudation rates of the basement during Mesozoic and Cenozoic times. Assuming a geothermal gradient of around 25 °C/km (Sobel and Strecker, 2003; Löbens et al., 2011; Dávila and Carter, 2013) and the effective closure temperature of the AHe system (approximately 60 °C), the upper thermal boundary of the paleo-PRZA would have been located at 2300 m depth. A Mesozoic sedimentary cover can be excluded for basement samples taken in the Sierras de San Luis and Comechingones (Löbens et al., 2011), as well as for most samples presented in this study (see also Jordan et al., 1989; Carignano, 1999). Additional evidence for missing sedimentary cover comes from the fact that except of samples 51–08, no burial re-heating could be traced in our thermal models. Thus, the age of passage through the PRZA of those basement samples allow the calculation of very rough denudation rates for the Pampean basement. These rates vary between 0.010 and 0.024 km/Ma, which is close to those of Jordan et al. (1989) and Löbens et al. (2011). Those rates are considerably small (see Ahnert, 1970); therefore, we

consider quite stable conditions within the Sierras Pampeanas since samples passed through the PRZ_A in Jurassic to Cretaceous times.

4.5. Comparison of the northern and southern Pampean ranges

The thermochronological data from the Eastern and Western Sierras Pampeanas and the new data presented in this study (Figs. 7 and 8) suggest similarities as well as important differences concerning the thermal and structural evolution of these regions compared to that of the northern Pampean ranges (e.g. Sobel and Strecker, 2003; Mortimer et al., 2007).

Within both areas, onset of the thermochronological record happened during the Late Paleozoic. In the northern Pampean ranges, cooling and exhumation within the temperature interval of approximately 200 °C is probably related to erosion affecting a pronounced relief generated during former orogenic phases in the Paleozoic (e.g. Löbens et al., 2013), similar to the most westerly mountain ranges of the Western Sierras Pampeanas, i.e. the Sierra de Pie de Palo and the Sierra Valle Fértil, as well as the Sierra de Pocho in the Eastern Sierras Pampeanas. The onset of cooling concerning the temperature interval of the ranges farther in the south of the Sierras Pampeanas, i.e. the Sierra de Comechingones, the Sierra de San Luis, the Sierra del Gigante, the Sierra de Varela, and Cantera Green, is presumably caused by a Permo-Triassic compression (see above). This process probably also affected the region of the Sierra de Pie de Palo and the Sierra Valle Fértil, leading to further cooling and exhumation within these areas. Whether it also had an effect on the northern Pampean ranges cannot be excluded, but it is not very likely. Furthermore, this compressional phase is potentially related to a Permo-Triassic flat-slab subduction, as suggested by the decreasing ages of arc-related volcanism towards the east, shown by Ramos and Folguera (2009), which is analogous to the Andean flat-slab subduction (e.g. Barazangi and Isacks, 1976; Pardo Casas and Molnar, 1987; Smalley and Isacks, 1990; Cahill and Isacks, 1992; Löbens et al., 2011). However, since the north–south extension of this flat-slab segment was presumably restricted to the more southern parts of the recent Sierras Pampeanas, i.e. the Eastern and Western Pampean ranges, the most northern mountain ranges, e.g. the Sierra de Aconquija and the Cumbres Calchaquíes, were not affected.

The Mesozoic cooling and exhumation or burial re-heating in the northern and southern parts of the Sierras Pampeanas are mainly linked to rift events and the position of the individual ranges relative to the related rift basins. The Triassic rifting mainly affected the Western Sierras Pampeanas, and the thermochronological record also suggests considerable cooling activity, especially for the mountain ranges proximal to the rift; The Eastern Sierras Pampeanas and the northern Pampean ranges can be characterized by a period of more or less thermal stability during that time. In contrast, Cretaceous rifting generally affected the more easterly part of the Sierras Pampeanas (e.g. Rossello and Mozetic, 1999; Ramos et al., 2002), which also includes the Sierra de Aconquija and the Cumbres Calchaquíes in the north. Therefore, there was particular cooling and exhumation or burial re-heating in these regions, i.e. Sierra de Aconquija (Sobel and Strecker, 2003) and the Sierra del Gigante, respectively, during that time, whereas the westernmost exposures of the Sierras Pampeanas were less affected.

The most important differences between the northern Pampean ranges and the Western and Eastern Sierras Pampeanas concern the thermal evolution during the Paleogene and the Neogene. The basement in the former region was partly affected by burial re-heating during the Paleogene, which was presumably related to the early uplift of the Puna Plateau, accompanied by sedimentation

into foreland basins (e.g. Mortimer et al., 2007). Subsequently, the development of the modern topography, i.e. exhumation and uplift of the recent mountain ranges, dominantly occurred during the Neogene (e.g. Coughlin et al., 1998; Sobel and Strecker, 2003; Carrapa et al., 2005; Mortimer et al., 2007). Whether this is related to the Miocene flat-slab subduction of the Nazca Plate beneath the South American Plate (e.g. Barazangi and Isacks, 1976; Pilger, 1981; Jordan and Allmendinger, 1986), as previously generally proposed in the literature (e.g. González Bonorino, 1950; Ramos et al., 2002), is not constrained by thermochronological data. Therefore, it could be possible that there is a correlation between the uplift of the northern Pampean ranges and the shallowing of the Nazca Plate, but there is no clear thermochronological indication.

In contrast, thermochronological data and related cooling models suggest that the regions of the Eastern and Western Sierras Pampeanas have generally been characterized by cooling and exhumation to near-surface temperatures since the Late Cretaceous to Paleogene, and locally even earlier than Late Cretaceous (i.e. Sierra de Pocho). Thus, exhumation occurred considerably earlier than in the northern Pampean ranges. To what extent the Andean deformation during the Neogene contributed to the overall exhumation and uplift within these regions and whether these processes are linked to the Miocene flat-slab subduction is not clearly illuminated by the thermochronological data.

5. Conclusions

- Locally, the oldest cooling event occurred during the Carboniferous, which we relate to a period of orogenic collapse.
- New thermochronological data show pronounced cooling during Permian to Triassic times. We attribute this to a period of flat-slab subduction at these latitudes, which clearly shows a distinct propagation of cooling activity from the Southwestern Sierras Pampeanas to the east in Early to Middle Triassic times. Additional evidence comes from an eastward propagation of Late Paleozoic calc-alkaline magmatism from the Southern Central Andes to the Southwestern Sierras Pampeanas during that period.
- Cooling decelerated or stagnated during the Late Triassic until the Early Cretaceous. This is contemporaneous with two rift events affecting the Sierras Pampeanas. Burial re-heating and the reset of AHe ages is only observed in the Sierra del Gigante, which is related to Cretaceous sedimentary cover of the basement. This indicates that substantial sedimentary thicknesses were only accumulated along the narrow and spatially restricted Cretaceous rift basins, as well as the existence of topography during this time.
- Published and new thermochronological data from the Sierras Pampeanas indicate that cooling to near-surface temperatures occurred between the Late Cretaceous and the Paleogene. This strongly supports the idea that a positive topography already existed before Neogene flat-slab subduction. We conclude that the amount of uplift attributed to this event is overestimated by previous models. Instead, we suggest that the Andean flat-slab subduction just accentuated the pre-existing relief.
- AHe ages and denudation rates of the Sierras de San Luis and Comechingones, although initially not intended to date paleoland-surfaces, support the formation age of erosional surfaces suggested by geomorphological studies. Denudation rates are considerably small, varying between 0.010 and 0.024 km/Ma; hence, we consider quite stable conditions since samples passed through the PRZ_A in Jurassic to Cretaceous times.
- Since the extent of the Permo-Triassic flat-slab is not well known, an effect on the northern Pampean ranges cannot be

excluded, but, based on thermochronological data, it is not very likely. The Western and Eastern Sierras Pampeanas have generally been affected by exhumation to near-surface temperatures since Late Cretaceous to Paleogene times. In contrast, final cooling in the northern Pampean ranges, at least in the Sierra de Aconquija and Cumbres Calchaquíes, occurred during the Neogene.

Acknowledgement

The help of Emilio Ahumada and Mónica López de Luchi, alleviating our stay in Argentina, as well as André Steenken and Juan Antonio Palavecino assisting in the field was highly appreciated. This research project is financed by the German Science Foundation (DFG project SI 438/31-1). Field work done by FB was financially supported by the DAAD (project number 1461 D/08/48018). The authors thank Andres Folguera and an anonymous reviewer for their critical comments on the manuscript.

References

- Aceñolaza, G., Toselli, A.J., 1988. El Sistema de Famatina, Argentina: su interpretación como orógeno de margen continental activo. In: Vº Congreso Geológico Chileno, vol. 1, pp. A55–A67.
- Ahnert, F., 1970. Functional relationships between denudation, relief, and uplift in large, mid-latitude drainage basins. *Am. J. Sci.* 268 (3), 243–263. <http://dx.doi.org/10.2475/ajs.268.3.243>.
- Arriagada, C., Roperch, P., Mpodozis, C., Cobbold, P.R., 2008. Paleogene building of the Bolivian Orocline: tectonic restoration of the central Andes in 2-D map view. *Tectonics* 27 (6). <http://dx.doi.org/10.1029/2008TC002269>.
- Baldwin, S.L., Lister, G.S., 1998. Thermochronology of the South Cyclades Shear Zone, Ios, Greece: effects of ductile shear in the argon partial retention zone. *J. Geophys. Res.* 103, 7315–7336. <http://dx.doi.org/10.1029/97JB03106>.
- Barazangi, M., Isaacs, B.L., 1976. Spatial distribution of earthquakes and subduction of the Nazca plate beneath South America. *Geology* 4, 686–692.
- Battaglia, A.A.C., 1982. Descripción Geológica de las Hojas 13f, Rio Hondo; 13g, Santiago del estero; 14g, El Alto; 14h, Villa San Martín; 15g, Frias (Provincias de Santiago del estero, Catamarca y Tucumán), Buenos Aires.
- Benjamín, M.T., Johnson, N.M., Naeser, C.W., 1987. Recent rapid uplift in the Bolivian Andes: evidence from fission-track dating. *Geol. Boulder* 15 (7), 680–683.
- Bense, F.A., Wemmer, K., Löbens, S., Siegesmund, S., 2013b. Fault gouge analyses: K/Ar illite dating, clay mineralogy and tectonic significance – a study from the Sierras Pampeanas, Argentina. *Int. J. Earth Sci.* <http://dx.doi.org/10.1007/s00531-013-0956-7>.
- Bense, F.A., 2013. Multi-method Chronometric Constraints on the Thermal, Structural and Morphotectonic Evolution of the Eastern and Western Sierras Pampeanas with Special Emphasis on K-Ar Dating of Fault Gouges (PhD thesis, Georg-August-Universität Göttingen. Geowissenschaftliches Zentrum der Fakultät für Geowissenschaften und Geographie, Göttingen <http://hdl.handle.net/11858/00-1735-0000-0001-BB21-8>.
- Bodenbender, G., 1890. La cuenca del valle del Río Primero en Córdoba. Descripción geológica del Río Primero desde la Sierra de Córdoba hasta la Mar Chiquita. *Bol. Acad. Nacion. Cienc.* (12), 5–55.
- Bodenbender, G., 1895. Devónico y Gondwana en la República Argentina. *Bol. Acad. Nacion. Cienc.* 15 (2–3), 201–252.
- Bodenbender, G., 1905. La Sierra de Córdoba. Construcción geológica y productos minerales de aplicación. *Anal. Minist. Agric. Nación. Secci. Geol.* 1 (2), 1–146.
- Bodenbender, G., 1911. Constitución geológica de la parte meridional de la provincia de La Rioja y regiones limítrofes. República Argentina. *Bol. Acad. Nacion. Cienc.* 19 (1), 2–211.
- Brackebusch, L., 1891. Mapa geológico del interior de la República Argentina. Escala 1:1.000.000. Academia Nacional de Ciencias, Córdoba.
- Cahill, T., Isaacs, B.L., 1992. Seismicity and shape of the subducted Nazca Plate. *J. Geophys. Res.* 97 (B12), 17503. <http://dx.doi.org/10.1029/92JB00493>.
- Caminos, R., 1979. Sierras pampeanas noroccidentales; Salta, Tucuman, Catamarca, La Rioja y San Juan (The northwestern Pampean Ranges; Salta, Tucuman, Catamarca, La Rioja and San Juan). In: Turner, J.C. (Ed.), II Simposio de Geología Regional Argentina, vol. 1, pp. 225–291.
- Carignano, C., 1999. Late Pleistocene to recent climate change in Córdoba Province, Argentina: Geomorphological evidence. *Quatern. Int.* 57–58 (1), 117–134. [http://dx.doi.org/10.1016/S1040-6182\(98\)00054-8](http://dx.doi.org/10.1016/S1040-6182(98)00054-8).
- Carrapa, B., Adelmann, D., Hilles, G.E., Mortimer, E., Sobel, E.R., 2005. Oligocene range uplift and development of plateau morphology in the southern Central Andes. *Tectonics* 24 (4).
- Carrapa, B., Trimble, J.D., Stockli, D.F., 2011. Patterns and timing of exhumation and deformation in the Eastern Cordillera of NW Argentina revealed by (U-Th)/He thermochronology. *Tectonics* 30 (3). Citation TC3003.
- Costa, C.H., Vita-Finzi, C., 1996. Late Holocene faulting in the southeast Sierras Pampeanas of Argentina. *Geology* 24, 1127–1130.
- Costa, C.H., Machette, M.N., Dart, R., Bastías, H., Paredes, J., Perucca, L., Tello, G., Haller, K., 2000. Map and Database of Quaternary Faults and Folds in Argentina. International Lithosphere Program, USGS, p. 81. Open-file report 00-0108.
- Costa, C.H., Gardini, C.E., Ortiz Suárez, A., Chiesa, J., Ojeda, G., Rivarola, D., Strasser, E., Morla, P., Ulaco, J., Tognelli, G., Carugno Durán, A., Vinciguerra, H., Salas, D., 2001a. Hoja Geológica 3366-I San Francisco del Monte de Oro. Serv. Geol. Miner. Argent. Bull. 278, 82.
- Costa, C.H., Murillo, V.M., Sagripanti, G.L., Gardini, C.E., 2001b. Quaternary intraplate deformation in the southeastern Sierras Pampeanas, Argentina. *J. Seism.* 5, 399–409.
- Coughlin, T.J., O'Sullivan, P.B., Kohn, B., Holcombe, R.J., 1998. Apatite fission-track thermochronology of the Sierras Pampeanas, central western Argentina: implications for the mechanism of plateau uplift in the Andes. *Geol. Boulder* 26 (11), 999–1002.
- Criado Roque, P., Mombrú, C., Ramos, V.A., Yrigoyen, M.R., 1981. Estructura e interpretación tectónica. In: 8º Congreso Geológico Argentino, pp. 155–192.
- Dávila, F.M., Carter, A., 2013. Exhumation history of the Andean broken foreland revisited. *Geology* 41 (4), 443–446. <http://dx.doi.org/10.1130/G33960.1>.
- DeCelles, P.G., Carrapa, B., Horton, B.K., Starck, D., Gehrels, G.E., 2007. Implications of Paleogene foreland basin evolution in NW Argentina for timing of Andean orogenesis. *Eos Trans. Am. Geophys. Union* 88 (52). Abstract T34B-04.
- Donelick, R.A., Ketcham, R.A., Carlson, W.D., 1999. Variability of apatite fission-track annealing kinetics: II. Crystallographic orientation effects. *Am. Miner.* 84, 1224–1234.
- Ehlers, T.A., Farley, K.A., 2003. Apatite (U-Th)/He thermochronometry: methods and applications to problems in tectonic and surface processes. *Earth Planet. Sci. Lett.* 206, 1–14.
- Farley, K.A., 2000. Helium diffusion from apatite: general behavior as illustrated by Durango fluorapatite. *J. Geophys. Res.* 105, 2903–2914.
- Farley, K.A., 2002. (U-Th)/He dating: techniques, calibrations, and applications. *Rev. Miner. Geochem.* 47 (1), 819.
- Farley, K.A., Wolf, R.A., 1996. The effects of long alpha-stopping distances on (U-Th)/He ages. *Geochim. Cosmochim. Acta* 60 (21), 4223–4229.
- Forque, G., 1968. Bosquejo geológico de la Sierra de Malanzan, La Rioja (Geology of the Sierra de Malanzan, La Rioja). *Actas Jorn. Geol. Argent.* 1, 111–120.
- Gallagher, K., Brown, R., Johnson, C., 1998. Fission track analysis and its applications to geological problems. *Annu. Rev. Earth Planet. Sci.* 26, 519–572.
- Galbraith, R.F., Laslett, G.M., 1993. Statistical models for mixed fission track ages. *Nucl. Tracks Radiat. Meas.* 21, 459–470.
- Gardini, C.E., Schotselaar, B., Costa, C.H., 1996. Reactivation tectonics in the Sierras Pampeanas, a case study from the Sierra de El Gigante, San Luis, Argentina. In: Abstract Volume Geological Association of Canada, Canada, p. A33.
- Gardini, C.E., Costa, C.H., Schmidt, C.J., 1999. Estructura subsuperficial entre las sierras de Las Quijadas-El Gigante y la sierra de Villa General Roca, San Luis (Underground structures between Sierras Las Quijadas-El Gigante and Sierra Villa General Roca, San Luis). In: 14º Congreso Geológico Argentino, vol. 14, pp. 219–221.
- Gleadow, A.J.W., Fitzgerald, P.G., 1987. Uplift history and structure of the Transantarctic Mountains: new evidence from fission track dating of basement apatites in the Dry Valley area, southern Victoria Land. *Earth Planet. Sci. Lett.* 82, 1–14.
- Gonzalez, R.R., Aceñolaza, G., 1972. La Cuenca de deposición Neopaleozóica-mesozoica del oeste Argentino. Fundación e Instituto Miguel Lillo, Tucumán. Miscelánea 40, 629–643.
- González Bonorino, F., 1950. Lagunas problemas geológicas de las Sierras Pampeanas. *Rev. Asoc. Geol. Argent.* 5, 81–110.
- González Diaz, E.F., 1981. Geomorfología. In: Geología y Recursos Naturales de la Provincia de San Luis. 8º Congreso Geológico Argentino Relatorio, pp. 193–236.
- Gordillo, C.E., Lencinas, A., 1979. Sierras Pampeanas de Córdoba y San Luis, in: Segundo Simposio de Geología Regional Argentina. Academia Nacional de Ciencias, pp. 577–650.
- Gross, W., 1948. Cuadro tectónico del valle de Punilla. *Rev. Asoc. Geol. Argent.* 3 (2), 73–132.
- Gutscher, M.A., Spakman, W., Bijwaard, H., Engdahl, E., 2000. Geodynamics of flat subduction: seismicity and tomographic constraints from the Andean margin. *Tectonics* 19 (5), 814–833.
- Hongn, F., del Papa, C., Powell, J., Petrinovic, I., Mon, R., Deraco, V., 2007. Middle Eocene deformation and sedimentation in the Puna-Eastern Cordillera transition (23 degrees -26 degrees S); control by preexisting heterogeneities on the pattern of initial Andean shortening. *Geol. Boulder* 35 (3), 271–274.
- Hourigan, J.K., Reiners, P.W., Brandon, M.T., 2005. U-Th zonation-dependent alpha-ejection in (U-Th)/He chronometry. *Geochim. Cosmochim. Acta* 69 (13), 3349–3365.
- Hilley, G.E., Coutand, I., 2010. Links between topography, erosion, rheological heterogeneity, and deformation in contractional settings: Insights from the central Andes: from the trench to the arc: subduction along South America. *Tectonophysics* 495 (1–2), 78–92. <http://dx.doi.org/10.1016/j.tecto.2009.06.017>.
- Hurford, A.J., Green, P.F., 1983. The zeta age calibration of fission-track dating. *Chem. Geol.* 41, 285–317.
- Introcaso, A., Lion, A., Ramos, V.A., 1987. La estructura profunda de las Sierras de Córdoba. *Rev. Asoc. Geol. Argent.* 42, 117–178.

- Isacks, B.L., 1988. Uplift of the Central Andean Plateau and bending of the Bolivian Orocline. *J. Geophys. Res.* 93, 3211–3231.
- James, D.E., Sacks, I.S., 1999. Cenozoic formation of the Central Andes; a geophysical perspective. *Spec. Publ. Soc. Econ. Geol.* U.S. 7, 1–25.
- Jordan, T.E., Allmendinger, R.W., 1986. The Sierras Pampeanas of Argentina: a modern analogue of Rocky Mountain foreland deformation. *Am. J. Sci.* 286, 737–764.
- Jordan, T.E., Alonso, R.N., 1987. Cenozoic stratigraphy and basin tectonics of the Andes Mountains, 20 degrees –28 degrees south latitude. *AAPG Bull.* 71 (1), 49–64. <http://dx.doi.org/10.1306/94886D44-1704-11D7-8645000102C1865D>.
- Jordan, T.E., Isacks, B.L., Allmendinger, R.W., Brewer, J.A., Ramos, V.A., Ando, C.J., 1983. Andean tectonics related to geometry of subducted Nazca plate. *Geol. Soc. Am. Bull.* 94 (3), 341–361.
- Jordan, T.E., Zeitler, P., Ramos, V.A., Gleadow, A.J.W., 1989. Thermochronometric data on the development of the basement peneplain in the Sierras Pampeanas, Argentina. *J. South Am. Earth Sci.* 2 (3), 207–222.
- Kay, S.M., Coira, B.L., 2009. Shallowing and steepening subduction zones, continental lithospheric loss, magmatism, and crustal flow under the Central Andean Altiplano-Puna Plateau. *Mem. Geol. Soc. Am.* 204, 229–259.
- Ketcham, R.A., Donelick, R.A., Carlson, W.D., 1999. Variability of apatite fission-track annealing kinetics: III. Extrapolation to geological time scales. *Am. Miner.* 84, 1235–1255.
- Ketcham, R.A., 2005. Forward and inverse modelling of low-temperature thermochronometry data. *Rev. Miner. Geochem.* 58, 275–314.
- Kleiman, L.E., Japas, M.S., 2009. The Choiyoi volcanic province at 34°S–36°S (San Rafael, Mendoza, Argentina): Implications for the Late Palaeozoic evolution of the southwestern margin of Gondwana. *Tectonophys.* 473 (3–4), 283–299. <http://dx.doi.org/10.1016/j.tecto.2009.02.046>.
- Koukharshky, M., Tassinari, C., de Brodtkor, Milka K., Leal, P., 2001. Basaltos del Neopaleozoico-Triásico temprano? en las sierras Norte de Córdoba y de Ambargasta, Sierras Pampeanas Orientales; petrografía y edades K/Ar (Neopaleozoic-Lower Triassic basalts of the Norte de Córdoba Sierras-Ambargasta (eastern Sierras Pampeanas); petrography and K/Ar ages). *Rev. Asoc. Geol. Argent.* 56 (3), 400–403.
- Laslett, G.M., Green, P.F., Duddy, I.R., Gleadow, A.J.W., 1987. Thermal annealing of fission tracks in apatite. *Chem. Geol. Isot. Geosci. Sect.* 65 (1), 1–13.
- Lencinas, A., Timonier, A., 1968. Algunas características estructurales del valle de Punilla, Córdoba (Structural characteristics of Punilla valley, Córdoba). *Actas Jorn. Geol. Argent.* 1, 195–207.
- Löbens, S., Bense, F.A., Wemmer, K., Dunkl, I., Costa, C.H., Layer, P., Siegesmund, S., 2011. Exhumation and uplift of the Sierras Pampeanas: preliminary implications from K–Ar fault gouge dating and low-T thermochronology in the Sierra de Comechingones (Argentina). *Int. J. Earth Sci.* 100 (2–3), 671–694. <http://dx.doi.org/10.1007/s00531-010-0608-0>.
- Löbens, S., Sobel, E.R., Bense, F.A., Wemmer, K., Dunkl, I., Siegesmund, S., 2013. Refined thermochronological aspects of the Northern Sierras Pampeanas. *Tectonics* 32 (3), 453–472. <http://dx.doi.org/10.1002/tect.20038>.
- Löbens, S., 2013. The Structural and Morphotectonical Evolution of the Sierras Pampeanas Constrained by a Multichronometrical Approach (PhD thesis). Georg-August-Universität Göttingen. Geowissenschaftliches Zentrum, Göttingen. <http://hdl.handle.net/11858/00-1735-0000-0015-A35E-A>.
- Lucero Michaut, N.H., Olsacher, J., 1981. Descripción Geológica de la hoja 19h. Cruz del Eje, provincia de Córdoba, Buenos Aires.
- Martínez, A., Rodríguez Blanco, L., Ramos, V.A., 2006. Permo-Triassic magmatism of the Choiyoi Group in the cordillera Frontal of Mendoza, Argentina: geological variations associated with changes in Paleo-Benioff zone. In: Backbone of the Americas Symposium, Mendoza. Asociación Geológica Argentina & Geological Society of America.
- Massabie, A., 1987. Neotectónica y sismicidad en la región de Sierras Pampeanas Orientales, sierras de Córdoba, Argentina. In: 10º Congreso Geológico Argentino, Actas 1, pp. 271–274.
- Miller, H., Söllner, F., 2005. The Famatina complex (NW Argentina): back-docking of an island arc or terrane accretion? Early Palaeozoic geodynamics at the western Gondwana margin. *Geol. Soc. Lond. Spec. Publ.* 246 (1), 241–256.
- Miró, R., Martos, D., 1999. Mapa Geológico De La Provincia De San Luis; Escala 1: 500.000. Instituto de Geología y Recursos Minerales & Servicio Geológico Minero Argentino, Buenos Aires.
- Mirré, J.C., 1976. Descripción Geológica de la Hoja 19e, Valle Fértil, Provincias de San Juan y La Rioja. Serv. Geol. Nacion. Bol. 147, 1–70. Buenos Aires.
- Mortimer, E., Carrapa, B., Coutand, I., Schoenbohm, L., Sobel, E.R., Sosa, G.J., Strecker, M.R., 2007. Fragmentation of a foreland basin in response to out-of-sequence basement uplifts and structural reactivation; El Cajón-Campo del Arenal Basin, NW Argentina. *Geol. Soc. Am. Bull.* 119, 637–653. <http://dx.doi.org/10.1130/B25884.1>.
- Mpodozis, C., Ramos, V.A., 1990. The Andes of Chile and Argentina. In: Ericksen, G.E., Canas Pinchet, M.T., Reinemud, J.A. (Eds.), *Geology of the Andes and its Relation to Hydrocarbon and Mineral Resources*, vol. 11, pp. 59–90.
- Mpodozis, C., Kay, S.M., 1990. Provincias magmáticas ácidas y evolución tectónica de Gondwana; Andes chilenos, 28–31 degrees S (Acidic magmatic provinces and the tectonic evolution of Gondwana; Chilean Andes, 28–31 degrees S). *Rev. Geol. Chile* 17 (2), 153–180.
- Müller, M.J., 1996. *Handbuch ausgewählter Klimastationen der Erde*, fifth ed. Universität Trier FB VI, Trier, p. 400.
- Noble, D.C., McKee, E.H., Mourier, T., Megard, F., 1990. Cenozoic stratigraphy, magmatic activity, compressive deformation, and uplift in northern Peru. *Geol. Soc. Am. Bull.* 102 (8), 1105–1113. [http://dx.doi.org/10.1130/0016-7606\(1990\)102<1105:CSMADC>2.3.CO;2](http://dx.doi.org/10.1130/0016-7606(1990)102<1105:CSMADC>2.3.CO;2).
- Oncken, O., Hindle, D., Kley, J., Elger, K., Victor, P., Schemmann, K., 2006. Deformation of the Central Andean Upper Plate System; Facts, Fiction, and Constraints for Plateau Models.
- Otamendi, J.E., Vujovich, G.I., de la Rosa, J.D., Tibaldi, A.M., Castro, A., Martino, R.D., 2009. Geology and petrology of a deep crustal zone from the Famatinian paleoarc, Sierras Valle Fértil-la Huerta, San Juan, Argentina. *J. South Am. Earth Sci.* 27, 258–279.
- Pardo Casas, F., Molnar, P., 1987. Relative Motion of the Nazca (Farallon) and South American Plates since late Cretaceous time. *Tectonics* 6 (3), 233–248.
- Pilger, R.H., 1981. Plate reconstruction, aseismic ridges, and low-angle subduction beneath the Andes. *Geol. Soc. Am. Bull.* 92, 448–456.
- Pilger, R.H., 1984. Kinematics of the South American subduction zone from global plate reconstructions. In: *Geodynamics of the Eastern Pacific Region, Caribbean and Cotia Arcs. Geodynamic Series*, vol. 9. American Geophysical Union, Washington D.C., pp. 113–125.
- Rabassa, J., Carignano, C., Cioccale, M., 2010. Gondwana Paleosurfaces in Argentina: an introduction. *Geociências* 29 (4), 439–466.
- Ramos, V.A., Escayola, M.P., Mutti, D., Vujovich, G., 2001. Proterozoic – early Paleozoic ophiolites in the Andean basement of southern South America. In: *Ophiolites and Oceanic Crust: New insights from Field Studies and Ocean Drilling Program*. Geological Society of America, pp. 331–349. Special Paper 349.
- Ramos, V.A., Folguera, A., 2009. Andean flat-slab subduction through time. *Geol. Soc. Lond. Spec. Publ.* 327 (1), 31–54. <http://dx.doi.org/10.1144/SP327.3>.
- Ramos, V.A., Jordan, T.E., Allmendinger, R.W., Mpodozis, C., Kay, S.M., Cortés, J.M., Palma, M., 1986. Paleozoic terranes of the Central Argentine–Chilean Andes. *Tectonics* 5 (6), 855–880.
- Ramos, V.A., Cristallini, E.O., Pérez, D., 2002. The Pampean flat-slab of the central Andes. *J. South Am. Earth Sci.* 15, 59–78.
- Ramos, V.A., 1982. Descripción geológica de la Hoja 20f Chepes, provincia de La Rioja.
- Ramos, V.A., 1988. Late Proterozoic–Early Paleozoic of South America – a collision history. *Episodes* 11, 168–174.
- Ramos, V.A., 2008. The basement of the Central Andes: the Arequipa and related terranes. *Annu. Rev. Earth Planet. Sci.* 36 (1), 289–324. <http://dx.doi.org/10.1146/annurev.earth.36.031207.124304>.
- Ramos, V.A., 2010. The Grenville-age basement of the Andes. *J. South Am. Earth Sci.* 29 (1), 77–91. <http://dx.doi.org/10.1016/j.jjsames.2009.09.004>.
- Reiners, P.W., Brandon, M.T., 2006. Using Thermochronology to understand orogenic erosion. *Annu. Rev. Earth Planet. Sci.* 34, 419–466.
- Reiners, P.W., Spell, T.L., Nicolescu, S., Zanetti, K.A., 2004. Zircon (U-Th)/He thermochronometry; He diffusion and comparisons with (super 40) Ar/(super 39) Ar dating. *Geochim. Cosmochim. Acta* 68 (8), 1857–1887. <http://dx.doi.org/10.1016/j.gca.2003.10.021>.
- Rossello, E., Mozetic, M.E., 1999. Caracterización estructural y significado geotectónico de los depocentros creacíos continentales del centro-este argentino. In: 5º Simposio sobre o Cretaceo do Brasil, Boletim 5, pp. 107–113.
- Rovereto, G., 1911. Studi di geomorfologia Argentina. I, La Sierra di Córdoba. E. Cuggiani, Roma.
- Salfity, J.A., Gorustovich, S.A., 1983. Paleogeografía del Grupo Paganzo (Paleozoico Superior). *Rev. Asoc. Geol. Argent.* 38, 437–453.
- Santa Cruz, E.O., 1979. Geología de las unidades sedimentarias aflorantes en el área de las cuencas de los ríos Quinto y Conlara, provincia de San Luis, República Argentina (Geology of sedimentary units outcropping in the region of the Quinto and Conlara river, Argentina), pp. 335–349.
- Schmidt, C.J., Astini, R.A., Costa, C.H., Gardini, C.E., Kraemer, P.E., 1995. Cretaceous rifting, alluvial fan sedimentation, and Neogene inversion, southern Sierras Pampeanas, Argentina. In: Tankard, A.J., Suárez Soruco, R., Welsink, H.J. (Eds.), *Petroleum Basins of South America*. Am. Assoc. Petr. Geol. Mem., 341–358.
- Simpson, C., Whitmeyer, S.J., Paor, D.G., de Gromet, L.P., Miró, R., Krol, M.A., Short, H., 2001. Sequential ductile to brittle reactivation of major fault zones along the accretionary margin of Gondwana in Central Argentina. *Geol. Soc. Lond. Spec. Publ.* 186 (1), 233–255. <http://dx.doi.org/10.1144/GSL.SP.2001.186.01.14>.
- Smalley Jr., R.F., Isacks, B.L., 1990. Seismotectonics of thin- and thick-skinned deformation in the Andean foreland from local network data; evidence for a seismogenic lower crust. *J. Geophys. Res.* 95, 12,487–12,498.
- Sobel, E.R., Strecker, M.R., 2003. Uplift, exhumation and precipitation: tectonic and climate control of late Cenozoic landscape evolution in the northern Sierras Pampeanas, Argentina. *Basin Res.* 15, 431–451.
- Stauder, W., 1973. Mechanism and spatial distribution of Chilean earthquakes with relation to subduction of the oceanic plate. *J. Geophys. Res.* 78, 5033.
- Steenken, A., Wemmer, K., López de Luchi, M.G., Siegesmund, S., Pawlig, S., 2004. Crustal provenance and cooling of the basement complexes of the Sierra de San Luis: an insight into the tectonic history of the pro to-Andean margin of Gondwana. *Gondwana Res.* 7 (4), 1171–1195. [http://dx.doi.org/10.1016/S1342-937X\(05\)71092-3](http://dx.doi.org/10.1016/S1342-937X(05)71092-3).
- Stelzner, A., 1885. Beiträge zur Geologie und Paläontologie der Argentinischen Republik und des angrenzenden, zwischen dem 32° u. 33° S. Br. gelegenen Teiles der Chilenischen Cordillere. I. Geologischer Theil, Cassel & Berlin, 329 pp.
- van der Pluijm, B.A., Marshak, S., 2004. *Earth Structure: an Introduction to Structural Geology and Tectonics*, second ed. W.W. Norton, New York, xvi, p. 656.

- van Gosen, W., 1998. Transpressive deformation in the southwestern part of the Sierra de San Luis (Sierras Pampeanas, Argentina). *J. South Am. Earth Sci.* (3), 233–264.
- Varela, R., Cingolani, C.A., Dalla Salda, L., Aragon, E., Teixeira, W., 1993. Las monzodioritas y monzogabros de Cacheuta, Mendoza; edad, petrología e implicancias tectónicas (The monzodiorites and monzogabbros of Cacheuta, Mendoza; age, petrology and tectonic implications). *Actas Congr. Geol. Argent.* 12 (4), 75–80.
- Vujovich, G.I., Godeas, M., Marín, G., Pezzutti, N., 1996. El complejo magmático de la Sierra de La Huerta, Provincia de San Juan. In: *Actas XIII Congreso Geológico Argentino y III Congreso de Exploración de Hidrocarburos*, vol. 3, pp. 465–475.
- Wolf, R.A., Farley, K.A., Silver, L.T., 1996. Helium diffusion and low-temperature thermochronometry of apatite. *Geochim. Cosmochim. Acta* 60 (21), 4231–4240. [http://dx.doi.org/10.1016/S0016-7037\(96\)00192-5](http://dx.doi.org/10.1016/S0016-7037(96)00192-5).
- Wolf, R.A., Farley, K.A., Kass, D.M., 1998. Modeling of the temperature sensitivity of the apatite (U-Th)/He thermochronometer. *Chem. Geol.* 148 (1–2), 105–114.
- Yañez, G., Ranero, G.R., Huene, R., von, Díaz, J., 2001. Magnetic anomaly interpretation across a segment of the Southern Central Andes (32–34°S): implications on the role of the Juan Fernández Ridge in the tectonic evolution of the margin during upper Tertiary. *J. Geophys. Res.* 106, 6325–6345.
- Yrigoyen, M.R., 1975. La edad Cretácica del Grupo Gigante (San Luis), su relación con cuencas circunvecinas. In: *Actas 2, 1º Congreso Geológico Argentino de Paleontología y Bioestratigrafía*, pp. 9–56.